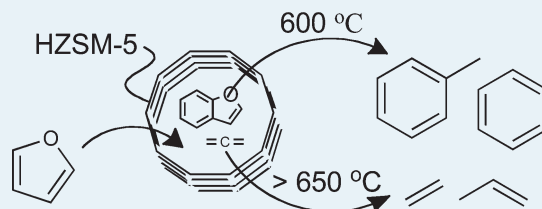


Chemistry of Furan Conversion into Aromatics and Olefins over HZSM-5: A Model Biomass Conversion Reaction

Yu-Ting Cheng and George W. Huber*

Department of Chemical Engineering, 159 Goessmann Lab, University of Massachusetts—Amherst, 686 North Pleasant Street, Amherst, Massachusetts 01003-9303, United States

ABSTRACT: The conversion of furan (a model of cellulosic biomass) over HZSM-5 was investigated in a thermogravimetric analysis–mass spectrometry system, in situ Fourier transform infrared analysis, and in a continuous-flow fixed-bed reactor. Furan adsorbed as oligomers at room temperature with a 1.73 of adsorbed furan/Al ratio. These oligomers were polycyclic aromatic compounds that were converted to CO, CO₂, aromatics, and olefins at temperatures from 400 to 600 °C. Aromatics (e.g., benzene, toluene, and naphthalene), oligomer isomers (e.g., benzofuran, 2,2-methylenebisfuran, and benzodioxane), and heavy oxygenates (C₁₂₊ oligomers) were identified as intermediates formed inside HZSM-5 at different reaction temperatures. During furan conversion, graphite-type coke formed on the catalyst surface, which caused the aromatics and olefins formation to deactivate within the first 30 min of time on-stream. We have measured the effects of space velocity and temperature for furan conversion to help us understand the chemistry of biomass conversion inside zeolite catalysts. The major products for furan conversion included CO, CO₂, allene, C₂–C₆ olefins, benzene, toluene, styrene, benzofuran, indene, and naphthalene. The aromatics (benzene and toluene) and olefins (ethylene and propylene) selectivity decreased with increasing space velocity. Unsaturated hydrocarbons such as allene, cyclopentadiene, and aromatics selectivity increased with increasing space velocity. The product distribution was selective to olefins and CO at high temperatures (650 °C) but was selective to aromatics (benzene and toluene) at intermediate temperatures (450–600 °C). At low temperatures (450 °C), benzofuran and coke contributed 60% of the carbon selectivity. Several different reactions were occurring for furan conversion over zeolites. Some important reactions that we have identified in this study include Diels–Alder condensation (e.g., two furans form benzofuran and water), decarbonylation (e.g., furan forms CO and allene), oligomerization (allene forms olefins and aromatics plus hydrogen), and alkylation (e.g., furan plus olefins). The product distribution was far from thermodynamic equilibrium.



KEYWORDS: furan, catalytic fast pyrolysis, biomass, aromatics, olefins, zeolites, HZSM-5, hydrocarbon pool

1. INTRODUCTION

Due to its low cost and availability, lignocellulosic biomass is receiving significant attention worldwide as a feedstock for renewable liquid fuels.^{1–4} Lignocellulosic biomass is not currently used as a feedstock to make liquid fuels due to technological and economic challenges.^{1,4} Several different processes for obtaining biofuels from biomass are currently under development.^{5,6} The ideal process to produce biofuels from lignocellulosic biomass would be a single step reactor at short residence times where solid biomass is directly converted into a liquid fuel. Catalytic fast pyrolysis (CFP) is a promising process that occurs in a single reactor at short residence times with solid biomass being directly converted into gasoline-range aromatics.^{7–9} In CFP, solid biomass is first pyrolyzed in the presence of a zeolite catalyst. The biomass is rapidly heated (>500 °C/s) to intermediate temperatures (400–600 °C) in the first step. The importance of pyrolysis heating rate is well-known.^{10,11} The biomass feedstock decomposes into pyrolysis vapors at these temperatures. The pyrolysis vapors then enter the zeolite pores, in which they are converted into aromatics, CO, CO₂, H₂O, and dehydrated oxygenates (furan and furfural).^{7,10–18}

Biomass consists of hydrogen-deficient compounds.^{19,20} The goal of biomass conversion processes is to reject oxygen as a

combination of CO, CO₂, and water and produce hydrocarbon products that have an enriched hydrogen and lower oxygen content. An effective hydrogen-to-carbon ratio (H/C_{eff}) can be used to help explain the hydrogen deficiency of biomass. The H/C_{eff} is defined as eq 1, where H, C, and O are the moles of hydrogen, carbon, and oxygen, respectively.^{19,20} Our research group has shown that the product yield from zeolite conversion of different biomass feedstocks is a function of the H/C_{eff} ratio, with higher yields being obtained with feedstocks of higher H/C_{eff} ratio.²¹

$$H/C_{\text{eff}} = \frac{H - 2O}{C} \quad (1)$$

The H/C_{eff} ratio of biomass-derived oxygenates is lower than that of petroleum-derived feedstocks due to the high oxygen content in biomass-derived compounds. The H/C_{eff} ratio of petroleum-derived feeds ranges from ~2 for highly paraffinic feeds to slightly greater than 1 for feeds with high aromatic content. The H/C_{eff} ratio of biomass-derived feedstock such as cellulose and glycerol are 0 and 0.67, respectively.

Received: February 24, 2011

Revised: April 18, 2011

Published: April 26, 2011

Zeolites offer one potential method for the conversion of hydrogen-poor biomass into fuels and chemicals. Researchers have used zeolites to directly convert biomass-derived carbohydrates into aromatics and olefins, beginning first in, the early 1980s with the work of Chen et al.^{20,22} Chen et al. fed sugars such as glucose and xylose, over HZSM-5 catalyst and produced aromatics in low yields (<5 wt %). Several researchers have used zeolite catalysts for the conversion of pyrolysis oils.^{23–27} Adjaye et al.^{23,24} reported that pyrolysis oil can be upgraded to produce hydrocarbons over HZSM-5 catalyst in a fixed-bed microreactor with aromatic yields up to 27 wt %. Sharma and Bakhshi²⁷ also used an HZSM-5 fixed-bed reactor to upgrade maple wood pyrolysis oil and obtained aromatic yields similar to those of Adjaye et al. Gayubo et al.²⁵ found that oxygenates, such as furan and furfural are responsible for coke formation during the pyrolysis oil upgrading. Recently, Corma and co-workers have studied the conversion of sorbitol and glycerol to aromatics and olefins over a series of different zeolite catalysts.¹⁹ They reported that HZSM-5 was the most selective catalyst to make aromatics and olefins. In 1988, Haniff and Dao used HZSM-5 to convert glucose, fructose, and their derivatives in which hydroxyl groups were replaced by ether bonds.²² They found that either homogeneous tar or catalytic tar has high (>40%) oxygen contents. The tar can be formed from furan-like intermediates. Increasing the H/C_{eff} ratio in feeds by adding methanol, or increasing reaction temperatures can reduce tar formation and increase aromatic yields. Horne and Williams also used HZSM-5 to catalytically pyrolyze woods, bio-oils, and vapors in the 1990s.^{28–30} In their study, furans and other oxygenates such as phenols were found in the liquid products, suggesting that these furans are important reaction intermediates during zeolite deoxygenation. Resasco et al. have used HZSM-5 catalyst to convert propanal, a “representative biomass-derived oxygenate”, into aromatics.^{31–33} The conversion pathway involves aldol condensation to form propanal dimer and trimer.³¹ They also demonstrated that the addition of mesopores into HZSM-5 catalyst was able to overcome diffusion limitation and coking reaction for propanal conversion, which are major concerns for biomass conversion over zeolites.³²

We have previously shown that both furfural and furan were major intermediates from CFP of glucose and cellulose at 600 °C.^{7,12} These products can account for up to 40% of the carbon in the oxygenated products.^{7,12} Furfural, furan, glucose, and cellulose all had similar aromatic product distribution for CFP.³⁴ This indicates that furan is most likely an important reaction intermediate for the CFP of biomass. In addition, both furan and furfural are thermally stable molecules that do not decompose in the gas phase, unlike glucose or cellulose. Furan can only be thermally decomposed into CO and allene with low yield (<5%) at temperatures higher than 900 °C.^{35,36} Therefore, furan is a good model compound and an important intermediate for biomass conversion by CFP.

Grandmaison et al. has studied the conversion of furan and furfural with HZSM-5 at low temperatures (<450 °C).³⁷ Furfural was converted into furan and condensed oxygenates such as benzofuran; however, most of the products were polymers. Kraushaar et al. hydrodeoxygenated furan over HZSM-5 and Pt-ZSM-5 catalysts at 400 °C and low space velocity (WHSV = 0.5 h⁻¹) with hydrogen as the carrier gas.³⁸ With the existence of Pt impurity, hydrogen was utilized efficiently, and the chemistry was shifted to hydrogenation for Pt-ZSM-5 instead of Diels–Alder condensation for HZSM-5. Furfural and furan have

H/C_{eff} ratios of 0 and 0.5, respectively, which is similar to the H/C_{eff} ratio of lignocellulosic biomass. We have also performed isotopic studies for CFP of glucose and observed that the aromatic products contain a random distribution of carbon.³⁹ This indicates that the reaction proceeds through a hydrocarbon pool in which the carbon from the biomass loses its identity within the zeolite pores.

Although many researchers have used zeolites to convert biomass-derived feedstocks into aromatics, little is known about the catalytic chemistry. Model compounds can help understand this rather complicated catalytic zeolite chemistry. The objective of this paper is to understand the catalytic chemistry that occurs inside zeolites during CFP by using furan as a model biomass compound. We used a continuous flow fixed-bed reactor, an in situ FTIR, and thermogravimetric analysis (TGA) to understand this reaction chemistry. Understanding this reaction chemistry can give us insight into how to design more effective zeolite catalysts and reactors for the efficient utilization of our biomass resources.

2. EXPERIMENTAL SECTION

2.1. Material. Furan (Sigma-Aldrich, liquid phase, 99+%, bp. 31 °C) was used as a feedstock without any pretreatment. An HZSM-5 catalyst purchased from Zeolyst (CBV 3024E, SiO₂/Al₂O₃ = 30) was used as the catalyst for this study. The HZSM-5 catalyst was sieved to 425–800 μm. The catalyst was calcined at 600 °C in the flow reactor at 60 mL/min air flow (Airgas, compressed air, dehumidified by a drierite tube) for 5 h prior to all reactions. The amount of active site was assumed to be equal to the amount of aluminum in the HZSM-5 catalyst.

The following calculations were used in this paper:

$$\begin{aligned} \text{TOF of a product} &= \frac{\text{rate of carbon produced in the product (mol carbon/h)}}{\text{moles of active sites (mol)}} \end{aligned} \quad (2)$$

$$\text{TOF of furan} = \frac{\text{rate of furan consumed (mol carbon/h)}}{\text{moles of active site (mol)}} \quad (3)$$

$$\begin{aligned} \text{deactivation rate} &= \frac{\text{carbon yield of furan (} t \text{)} - \text{carbon yield of furan (} t = 0 \sim 1.5 \text{)}}{\text{carbon yield of furan (} t = 0 \sim 1.5 \text{)} \times t} \end{aligned} \quad (4)$$

$$\text{catalyst activity} = \frac{\text{current TOF of furan}}{\text{initial TOF of furan}} \quad (5)$$

2.2. Catalytic Conversion of Furan in the Flow Fixed-Bed Reactor. The catalytic reactions were carried out in a fixed-bed quartz reactor of 1/2 in. o.d. Sieved HZSM-5 powders were held in the reactor by a quartz frit. The reactor temperature was measured using a thermocouple inserted on top of the catalyst bed. Prior to reactions, the catalyst bed was calcined as described above. After calcination, the reactor was flushed by helium (Airgas, 99.999%) at 408 mL/min for 5 min and cooled down or heated up to reaction temperatures. The helium then was

switched to bypass the reactor, and the inlet and outlet valves of the reactor were closed. Furan was pumped into the helium stream by a syringe pump (Fisher, KDS100). Prior to the run, the furan bypassed the reactor for 30 min before switching the helium stream to go through the reactor. An air bath condenser was used to trap the heavy products. Gas phase products were collected by air bags. All runs were done at atmospheric pressure. No pressure drop was detected across the catalyst bed. After reaction, the reactor was flushed by helium at a flow rate of 408 mL/min for 45 s at the reaction temperature. The effluent was collected by an air bag. After reactions, the spent catalyst was regenerated at 600 °C under 60 mL/min air flow. The CO formed during regeneration was converted to CO₂ by a copper converter (copper oxide, CuO, Sigma-Aldrich) working at 240 °C. CO₂ was trapped by a CO₂ trap (Ascarite, Sigma-Aldrich). Coke yield was obtained by weighing the weight change of the CO₂ trap.

Finally, the reactor was cooled to room temperature. Condensed products were extracted by 10 mL of ethanol from the condensers to obtain the liquid products. Both liquid and gas products were identified by GC/MS (Shimadzu-2010) and quantified by GC/FID/TCD (Shimadzu 2014 for gas samples, and HP-7890 for liquid samples). To calibrate the GC/FID, gas-phase standards including C₂–C₆ normal olefins (Scott Specialty Gas, 1000 ppm for each olefin), furan, benzene, and toluene (Sigma-Aldrich, they can be vaporized in airbags); and liquid-phase standards, including xylenes, ethylbenzene, styrene, benzofuran, indene, and naphthalene (Sigma-Aldrich), were injected into the GC/FID. CO and CO₂ were quantified by GC/TCD. A standard CO and CO₂ mixture (Airgas, 14% CO and 6% CO₂, helium balance) was injected into GC/TCD to do the calibration. The sensitivity of other compounds was assumed to be proportional to the number of carbon in similar olefins and aromatics (e.g., allene vs propylene; methylindene vs indene). In our study, <0.05% carbon or the products was collected in the liquid trap. The majority of the products were in either the gas phase or coke deposited on the catalyst. Our carbon balances closed with 90% for all runs in this paper unless otherwise mentioned.

Standard reaction conditions for furan conversion in the flow fixed-bed reactor were 600 °C, WHSV 10.4 h⁻¹, and partial pressure 6 Torr unless otherwise noted. In this condition, the furan was pumped at a pumping rate of 0.58 mL/h, and the carrier gas was controlled at 408 mL/min. The amount of catalyst that was loaded into the reactor was typically 57 mg HZSM-5 powders.

2.3. Leaching Experiment. To determine the compounds retained inside HZSM-5 during furan conversion, we used the method introduced by Guisnet in 1989.⁴⁰ Spent catalyst was obtained by converting furan in the flow fixed-bed reactor at different temperatures. We dissolved spent catalyst in a 7.5 mL 20% hydrofluoric acid (HF) solution. The mixture was shaken and allowed to stand overnight. Organics were extracted by adding 5 mL dichloromethane (DCM). The organic phase solution was subjected to GC/MS, UV–vis (HP 8452A) and GPC (Shimadzu HPLC/UV; GPC column: Varian GPC/SEC column, mesopore, 300 × 7.5 mm; calibration standard, linear polystyrene) analysis to identify species forming intermediates and coke. Prior to GPC and UV–vis analysis, samples were diluted to 1/20 volumetric concentration by DCM. For the UV–vis analysis, transparenance mode was used. Diluted DCM solution was placed in a quartz cuvette and was irradiated by an UV–vis light. After passing through the cuvette, the UV–vis

light was detected by a detector. Pure DCM was used as the standard.

2.4. Temperature-Programmed Analysis. *2.4.1. TGA–MS.* Temperature-programmed results were qualitatively obtained by using TGA–MS and in situ FTIR instruments. Furan-saturated HZSM-5 powders were obtained by using the flow reactor system described in Section 2.2. The calcined HZSM-5 catalyst bed was subjected to a helium stream with 12 Torr furan for 1 h at room temperature. The furan-saturated HZSM-5 powders were subjected to TGA and in situ FTIR analysis.

A 34 mg portion of furan-adsorbed HZSM-5 powder was placed in an alumina pan and treated in flowing helium at 100 mL/min at 50 °C for 2 h in the TGA chamber (TGA: TA Instrument, SDT Q600) to remove weak adsorption. After pretreatment, the temperature was increased to 600 °C at a ramp rate of 50 °C/min under the same helium flow. The effluent was monitored by a mass spectroscopy where several ion fragments were continuously recorded. The calcined HZSM-5 powders without furan adsorbed were also subjected to the same process as a blank run.

A separate furan adsorption–desorption experiment was carried out in the TGA instrument. A 24 mg portion of calcined HZSM-5 was placed in the alumina pan and treated by 100 mL/min air flow at 600 °C for 1 h in the TGA chamber. After cooling down to 30 °C, the TGA chamber was flushed by 100 mL/min helium flow until it was stable (to remove the air in the TGA chamber). Adsorption measurement was carried out by introducing furan into a separate helium stream (30 mL/min) by a syringe pump at a pumping rate of 0.2 mL/h. After 1-h adsorption, the feeding of furan was stopped, but major helium flow for 30 min was continued to remove weak adsorption. Then the temperature was linearly increased to 600 °C (at 50 °C/min). The effluent was also monitored by mass spectroscopy to make sure the same products as previous runs were obtained. Finally, the gas flow was switched to dry air, and the temperature was held at 600 °C for 1 h to regenerate the catalyst and determine the amount of coke. By analyzing the weight-loss curve of the catalyst, the amount of furan adsorbed on an acid site can be obtained.

2.4.2. In Situ FTIR. Around 15 mg of furan-saturated HZSM-5 powder was placed in a microreactor, which was fixed in the FTIR diffraction chamber (FTIR: Bruker, Equinox 55; in situ microreactor: Harrick, HVC-DRP). The technique is well-known as DRIFT (diffraction-reflection infrared Fourier-transform). The microreactor was purged for 10 min at 60 mL/min helium flow to remove air and weak adsorption. After pretreatment, the temperature was jumped to various temperatures under 60 mL/min helium flow, and IR spectra were taken at each temperature. Prior to taking the spectra, the temperature was kept stable for 5 min. Each sample was subjected to 254 scans, and the resolution was 4 cm⁻¹. A separate run was done to obtain IR spectrum of pure HZSM-5. A 30 mg portion of HZSM-5 was calcined at 600 °C for 2 h at 60 mL/min air flow in the microreactor. The HZSM-5 IR spectrum then was taken at 600 °C after helium treatment. In these studies, KBr crystal powder was used as background.

Another in situ FTIR analysis was performed separately. We calcined HZSM-5 in the microreactor at 600 °C (air, 60 mL/min) and purged by helium (60 mL/min). A 60 μL portion of furan was dosed into the helium stream and was carried into the microreactor to produce a coked HZSM-5 sample. The coked HZSM-5 was calcined at 400 and 600 °C (air, 60 mL/min), and

the IR spectra were taken at each temperature to understand the thermal resistance of coke. In this run, pure, calcined HZSM-5 at 600 °C was used as the background.

2.4.3. Coke Combustion (Temperature-Programmed Oxidation, TPO). To understand the coke type, we adopted the method introduced by Gayubo.^{25,41} We produced spent catalyst in the flow fixed-bed reactor and regenerated it in the TGA chamber. The reaction conditions were the same as the standard reaction (WHSV 10.4 h⁻¹, partial pressure 6 Torr, temperature was varied). During regeneration, we increased the temperature at a ramp rate of 5 °C/min to 600 °C in the air atmosphere (100 mL/min). The temperature was kept at 600 °C for 30 min. The weight change of each sample was recorded once the temperature reached 50 °C.

3. RESULTS

3.1. Temperature-Programmed Analysis: TGA–MS. Furan was adsorbed at room temperature on the HZSM-5. The catalyst was originally white but turned red due to oligomerization of the furan after 10-min time on-stream, as shown in Figure 1. This was similar to the adsorption of thiophene on HZSM-5.^{42,43} Furan

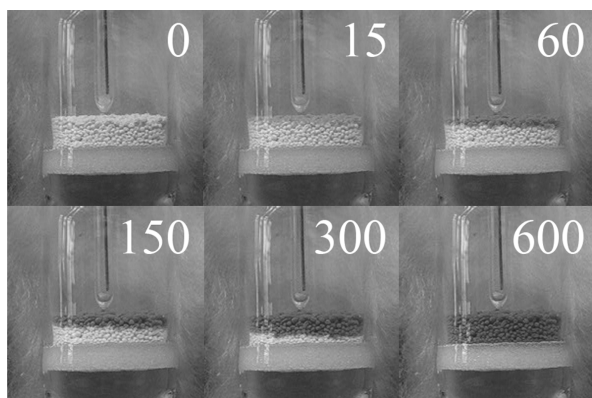


Figure 1. Furan adsorption on HZSM-5 catalyst at room temperature in a fixed-bed reactor for reaction times of 0, 15, 60, 150, 300, and 600 s. Furan partial pressure, 12 Torr; $W_{\text{HZSM-5}}$, 300 mg.

adsorption was continued for another 50 min to make sure that furan was completely saturated on the HZSM-5 powder. The dark red, furan-saturated HZSM-5 powder was then subjected to temperature-programmed desorption in the TGA instrument. Figure 2 shows the products that were desorbed from this powder. Water was mostly removed at temperatures lower than 200 °C, as shown by the first peak of weight loss. A separate run was performed using pure HZSM-5 that indicated the water released from furan-saturated HZSM-5 was from the furan feed, since no water was observed from the pure HZSM-5 catalyst. Some unreacted furan as well as CO, CO₂, and water desorbed at a temperature beginning around 200 °C. Aromatic and olefin products, including ethylene, benzene, and toluene, were formed around 500 °C. They were responsible for the weight loss at 500 °C. CO and CO₂ were detected throughout the entire experiment, with peak maximum around 450 and 370 °C, respectively. The CO and CO₂, as well as water removed at 450 °C, contributed the majority of weight loss from 350 to 450 °C. Finally, hydrogen and naphthalene were desorbed at 600 °C, which caused a shoulder in the weight loss curve at 600 °C. However, since the weight loss at 600 °C was small, and due to slow diffusion, naphthalene may form at the same temperatures as benzene and toluene. The release of hydrogen at 600 °C can be attributed to the formation of graphite-type coke that is a hydrogen-deficiency product.

In summary, at low temperatures (<400 °C), oxygen was extracted from furan oligomers via dehydration, decarbonylation and decarboxylation reactions to form certain intermediates remaining on the catalyst. These intermediates probably are oxygenated polymers.³⁷ At moderate temperatures (400–600 °C), the intermediates were converted to olefins and aromatics. More oxygen was removed at this temperature in the form of CO and CO₂. At high temperatures (600 °C), all hydrocarbons remained inside the HZSM-5-catalyst-formed coke, probably a graphite type that is a hydrogen deficiency product. The weight yield of coke was 20% after our TPD experiments. The coke contained oxygenates and graphite-type carbons. This will be discussed later in this paper.

These results were consistent with those of Chica et al.,^{43,44} who used a flow reactor and the TPD method to analyze the

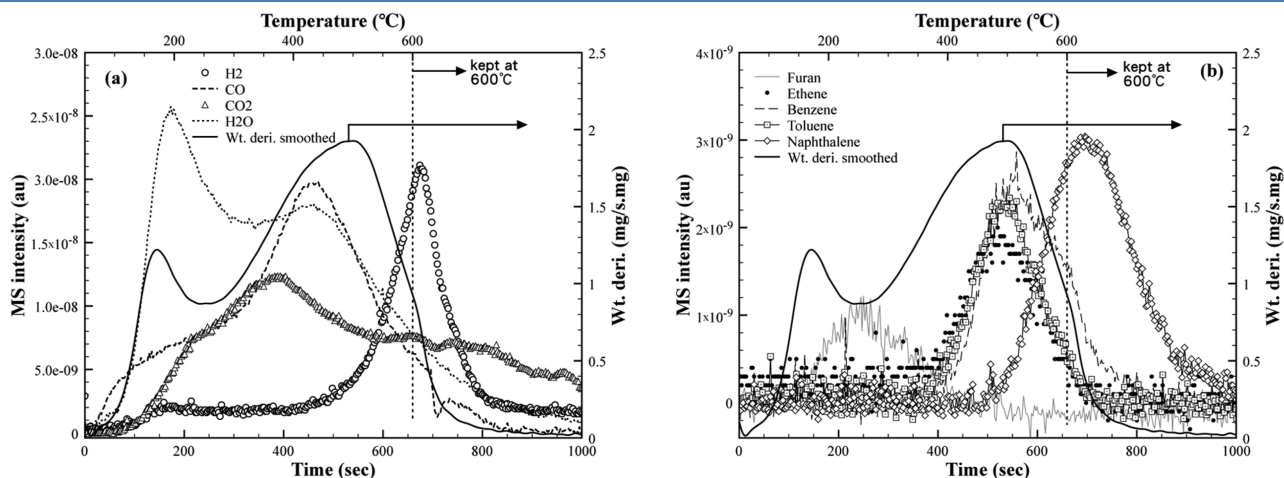


Figure 2. Temperature-programmed desorption of furan over HZSM-5. Furan was adsorbed at room temperature in the flow fixed-bed reactor. The TGA heating rate was 50 °C/s in flowing He. (a) MS intensity of hydrogen ($m/z = 2$), water ($m/z = 18$), CO ($m/z = 28$), and CO₂ ($m/z = 44$), and time derivative of sample weight. (b) MS intensity of furan ($m/z = 68$), ethylene ($m/z = 27$), benzene ($m/z = 78$), toluene ($m/z = 91$), and naphthalene ($m/z = 128$), and time derivative of sample weight.

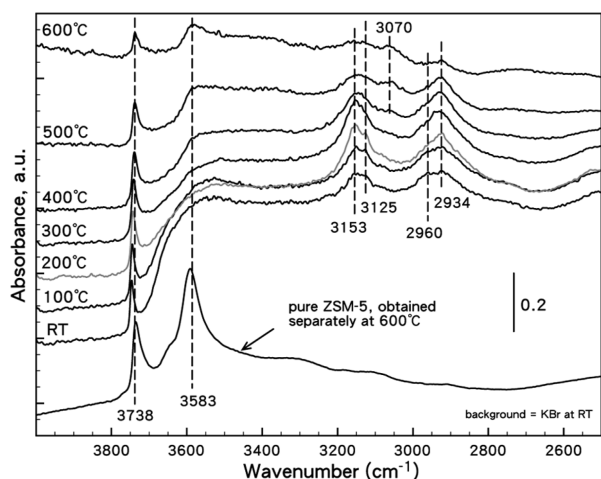


Figure 3. In-situ FTIR spectra of furan conversion over HZSM-5 catalyst. Furan adsorbed at room temperature in the flow fixed-bed reactor and was subjected to in situ FTIR analysis. During the FTIR analysis, the temperature was jumped to set points and held for 5 min at each temperature. Scan number, 254; resolution, 4 cm^{-1} . The microreactor was continuously purged by helium at 60 mL/min.

Table 1. FTIR Peak Assignments

wavenumber (cm^{-1})	assignment	assignment
3738	$\nu(\text{O}-\text{H})$	SiO-H
3583	$\nu(\text{O}-\text{H})$	Brønsted acid sites
3153, 3125	$\nu(\text{C}-\text{H})$	C-H stretching of C=C-H
3070	$\nu(\text{C}-\text{H})$	coke, aromatic
2960	$\nu(\text{C}-\text{H})$	C-H stretching of C-C-H, methyl group
2934	$\nu(\text{C}-\text{H})$	C-H stretching of C-C-H, methylene group

adsorption-desorption of thiophene on HZSM-5 catalyst. Thiophene was also adsorbed as spatially restricted oligomers on HZSM-5 with an adsorption uptake of thiophene to Al molar ratio ~ 1.7 . Spoto et al.⁴² used FTIR to show that furan, thiophene, and pyrrole were adsorbed as oligomers on HZSM-5 catalyst. In their UV-vis study, the adsorption of those compounds on HZSM-5 catalyst resulted in a red shift. The HZSM-5 color turned to red after adsorption. They also found that the sizes of polymers formed from pyrrole, furan, and thiophene were very similar (they claimed that no more than 3 monomers). The reason is that those molecules have similar kinetic diameters ($\sim 4.5\text{--}5.0$ Å), and their chain lengths are dependent on steric constraints imposed by HZSM-5 channels.⁴³ In our study, we found that furan also adsorbed as spatially restricted oligomers with a furan-to-aluminum molar ratio of 1.73, which is very close to the thiophene results of Chica et al. The chain length of these furan oligomers was restricted by HZSM-5 channels.

3.2. Temperature-Programmed Analysis: In Situ FTIR.

Figure 3 shows the IR spectra of furan conversion over HZSM-5 taken at different temperatures (O-H stretching region). Absorption bands are assigned as shown in Table 1.^{42,45–48}

Furan was polymerized on the HZSM-5 surface and led to the absorption at $3200\text{--}3100$ cm^{-1} and 2960 and 2934 cm^{-1} . The

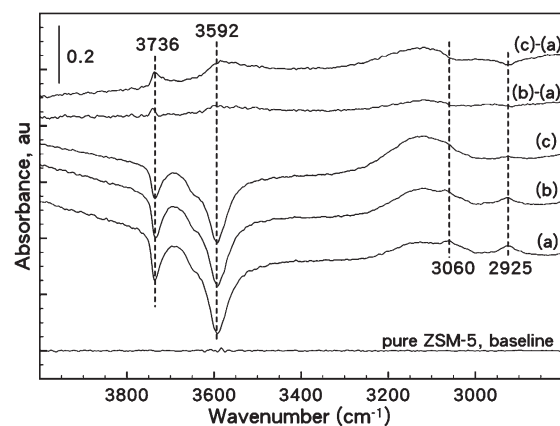


Figure 4. In-situ FTIR spectra taken during spent HZSM-5 regeneration. (a) Furan ($60\ \mu\text{L}$) adsorbed at $600\ ^\circ\text{C}$ (furan was carried by $60\ \text{mL}/\text{min}$ helium into the microreactor) and the spent catalyst was regenerated at $60\ \text{mL}/\text{min}$ air flow at (b) 400 and (c) $600\ ^\circ\text{C}$.

$3200\text{--}3100$ cm^{-1} stretch was assigned to the $\nu(\text{C}-\text{H})$ of $\text{C}=\text{C}-\text{H}$. The 2960 and 2934 cm^{-1} absorption was assigned to the $\nu(\text{C}-\text{H})$ of a methyl and methylene group, respectively.^{42,45} The absorption band at 3738 cm^{-1} was assigned to terminal silanols (SiO-H) that were weak Lewis acid sites and were slightly perturbed by furan adsorption.^{42,47,48} These same peaks have been observed by Spoto et al., who studied polyfuran adsorbed on the HZSM-5 surface.⁴² When the sample was heated up, the $3200\text{--}3100$ cm^{-1} band representing $\nu(\text{C}-\text{H})$ of $\text{C}=\text{C}-\text{H}$ increased at temperatures lower than $300\ ^\circ\text{C}$ and then slightly decreased at $400\ ^\circ\text{C}$. These results suggest that $\text{C}=\text{C}$ bonds were formed at low temperatures and then decomposed or desorbed at higher temperatures.

According to TGA-MS, the process of furan conversion may include dehydration, decarboxylation, and decarbonylation reactions. The absorption band from 3200 to 3100 cm^{-1} further decreased at $500\ ^\circ\text{C}$ and almost disappeared at $600\ ^\circ\text{C}$, suggesting that the rate of $\text{C}=\text{C}$ decomposition and desorption was faster than formation. A new absorption band at 3065 cm^{-1} was found from $400\ ^\circ\text{C}$, which is assigned to $\nu(\text{C}-\text{H})$ of an aromatic-structure coke (polycyclic aromatics, or graphite-type coke).⁴⁶ The absorption band at 2960 cm^{-1} (methyl group) formed at room temperature, decreased at $400\ ^\circ\text{C}$ and disappeared at $600\ ^\circ\text{C}$; however, the peak at 2934 cm^{-1} (methylene group) was more stable but still showed low intensity (not completely disappeared) at $600\ ^\circ\text{C}$. This suggested that there were no terminal methyl or methylene groups at $600\ ^\circ\text{C}$. This can be attributed to the formation of graphite-type coke in which all carbons were not terminal methyl or methylene carbons. According to TGA-MS, the earlier decrease in the methyl group can be attributed to the formation of olefins or other products that were removed from surface. Moreover, the significant decrease in methylene groups from 500 to $600\ ^\circ\text{C}$ was caused by the dehydrogenation reactions that formed graphite-type coke. As for the decrease in $\nu(\text{C}-\text{H})$ of $\text{C}=\text{C}-\text{H}$ at 3153 and 3125 cm^{-1} at $400\ ^\circ\text{C}$, it can be explained by the formation of highly conjugated double bonds (graphite-type coke) and being redshifted to 3070 cm^{-1} . The Brønsted acid site at 3590 cm^{-1} was restored a little bit, probably due to desorption of products.

In a separate run, the HZSM-5 at $600\ ^\circ\text{C}$ in the helium atmosphere was taken as the baseline. After introducing $60\ \mu\text{L}$ of

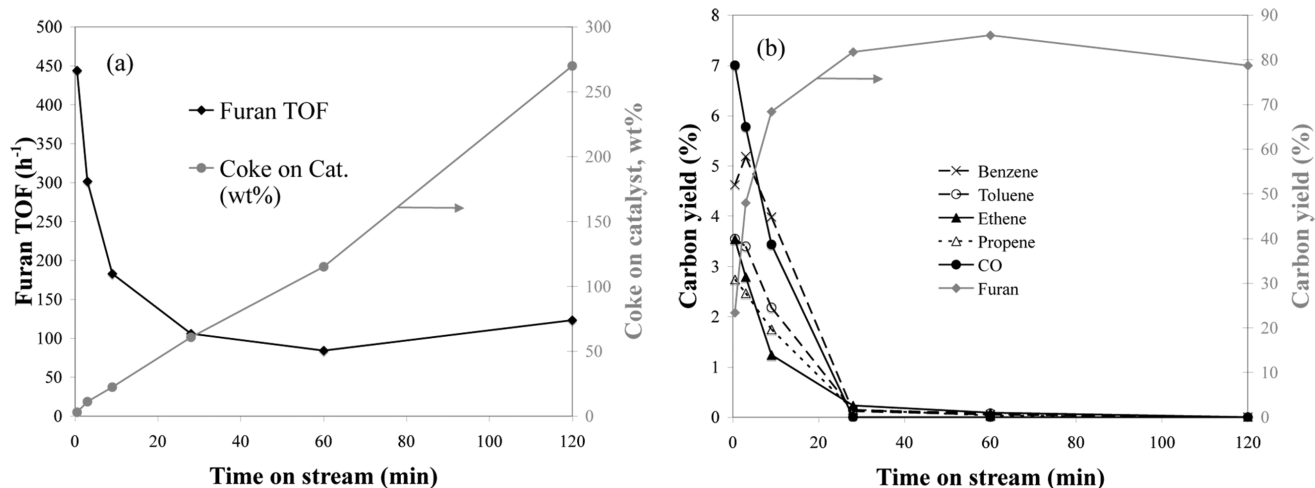


Figure 5. Furan conversion over HZSM-5 as a function of time on-stream (reaction conditions: temperature, 600 °C; furan partial pressure, 6 Torr; and space velocity, 10.4 h⁻¹).

furan in this condition, as shown in Figure 4, there are two peaks at 3736 and 3592 cm⁻¹, which were assigned to terminal silanols and Brønsted acid sites, respectively. The coke at 3060 cm⁻¹ can be removed only via regeneration in air at 600 °C. This was further evidence that the coke was a graphite-type which can only be removed by calcination at temperatures higher than 550 °C.^{25,49} Similar to Figure 3, the Brønsted acid sites were restored slightly, which led to a slight restoration of the negative peak at 3592 cm⁻¹ due to regeneration (see the subtraction b – a and c – a).

3.3. Catalyst Deactivation As a Function of Time on-Stream. Furan conversion was carried out using a fixed-bed reactor described in Section 2.2. During the reaction, the catalyst deactivated due to coke deposition on the catalyst surface. Figure 5 shows the evolution with time on-stream of the reaction rate and carbon yields of the selected products, including benzene, toluene, ethylene, propylene, and CO. These species plus coke contributed to 90% of the products. The other quantified products are shown in Table 2. We obtained >90% carbon balance and calculated the coke yield by assuming all unidentified carbons were coke. The catalyst continuously lost activity as the amount of coke increased on the catalyst surface. After 30-min time on-stream, the catalyst was nearly completely deactivated, with only furan being observed in the gas phase. However, the catalyst was still converting the furan into coke even after 2-h time on-stream. The furan conversion and coke accumulation were stable after 30-min on-stream. Table 2 also shows the normalized deactivation rate of the catalyst as defined by eq 4. The deactivation rate was initially very fast and gradually decreased, as the coke level increased. The rate of coke accumulation also decreased with time on-stream. However, the selectivity to coke increases with time on-stream. The carbon yield of most products was relatively stable during the first 3-min time on-stream, demonstrating that a pseudo-steady state can be obtained by testing the catalysts for short time period; however, the catalyst deactivated very rapidly and only coke was observed after 30 min time on-stream.

3.4. Effect of Space Velocity. We studied the effect of space velocity on the product distribution, as shown in Table 3. The WHSV was varied by adding different amounts of HZSM-5 catalyst to the reactor system. All data were collected at a short

time on-stream (4.5 min), at which point, on the basis of the product formation, no significant catalyst deactivation was observed. The furan conversion was varied from 0.28 to 0.97 by changing the WHSV from 21.86 to 1.95 h⁻¹. Carbon monoxide had the highest carbon selectivity of any product, with a selectivity from 11 to 18%. This suggests that the primary pathway for oxygen removal from furan was by decarbonylation. If all the oxygen is removed by decarbonylation, then the CO selectivity should be 25%. This suggests that other pathways also existed for oxygen removal. Other oxygenated products observed include CO₂, benzofuran, methylfuran, and also furylethylene. We also observed H₂O from the TGA–MS experiments, suggesting that dehydration was a pathway to remove oxygen, as well. We did not analyze for water in the products from the fixed-bed reactor. The selectivity of CO + CO₂ was only 12% at low furan conversion, suggesting some of the oxygen was present within the zeolite framework as unidentified oxygenates or as H₂O. The CO + CO₂ selectivity increased from 11.6 to 21.0% as the furan conversion increased from 28 to 97%, suggesting that the majority of the oxygen was removed as either CO or CO₂ at the higher conversion.

On the basis of carbon selectivity, we classified all identified products into product or intermediate. The “product” was the species whose selectivity increased with increasing furan conversion. The “products” were the final stable products. The “intermediate” was the species whose selectivity decreased with increasing furan conversion. CO, CO₂, benzene, toluene, xylenes, ethylene, and propylene were final products, since their selectivity increased with furan conversion. The carbon selectivity of these products decreased according to the following order: CO > ethylene ~ benzene ~ toluene > propylene > CO₂ ~ xylenes.

Intermediates that were identified in order of decreasing selectivity include coke ≫ indene > naphthalene ~ cyclopentadiene > styrene ~ benzofuran > allene ~ methylfuran ~ methylindene > methylindene ~ methylindene ~ indane > ethylbenzene ~ hexatriene ~ hexadienyne ~ furylethylene ~ methylstyrene ~ dihydronaphthalene. The coke selectivity decreased with increasing furan conversion. The “coke” may include compounds retained inside HZSM-5 pores, including intermediates such as benzofuran and indene. These results were consistent with results of TGA–MS in which furan adsorbed as oligomers on HZSM-5.

Table 2. Carbon Yield (%), Deactivation Rate, Catalyst Activity, and wt % of Coke on Catalyst As a Function of Time on-Stream^a

	time on-stream (min)					
	0–0.5	2.5–3	8.5–9	27.5–28	59.5–60	119.5–120
furan	23.40	47.97	68.42	81.74	85.50	78.73
CO	7.00	5.78	3.44	0.00	0.00	0.00
CO ₂	1.24	0.39	0.10	0.00	0.00	0.00
C ₂ H ₄ (ethylene)	3.54	2.79	1.24	0.23	0.09	0.00
C ₃ H ₆ (propylene)	2.74	2.47	1.75	0.15	0.03	0.00
C ₄ olefins	0.37	0.34	0.47	0.03	0.00	0.00
C ₆ H ₆ (benzene)	4.62	5.19	3.98	0.12	0.05	0.00
C ₇ H ₈ (toluene)	3.55	3.40	2.18	0.14	0.08	0.00
C ₈ H ₁₀ (ethylbenzene)	0.21	0.44	0.25	0.06	0.00	0.00
C ₈ H ₁₀ (xylenes)	0.71	0.81	0.21	0.09	0.00	0.00
C ₈ H ₈ (styrene)	0.76	0.48	0.19	0.05	0.00	0.00
C ₈ H ₆ O (benzofuran)	0.14	0.13	0.08	0.03	0.02	0.00
C ₉ H ₈ (indene)	0.65	0.49	0.26	0.09	0.07	0.03
C ₁₀ H ₈ (naphthalene)	0.41	0.17	0.09	0.08	0.07	0.00
C ₃ H ₄ (allene)	0.31	0.33	0.39	0.21	0.10	0.00
C ₅ H ₆ (cyclopentadiene)	0.60	1.24	0.76	0.04	0.00	0.00
C ₅ H ₆ O (methylfuran)	0.07	0.38	0.42	0.05	0.02	0.00
C ₆ H ₈ (hexatrienes)	0.19	0.11	0.08	0.00	0.00	0.00
C ₆ H ₆ (hexadienyne)	0.05	0.10	0.08	0.04	0.00	0.00
C ₆ H ₆ O (furylthylene)	0.00	0.06	0.02	0.00	0.00	0.00
C ₉ H ₁₂ (trimethylbenzene)	0.05	0.06	0.06	0.12	0.00	0.05
C ₉ H ₁₀ (methylstyrene)	0.06	0.08	0.03	0.00	0.00	0.00
C ₉ H ₁₀ (Indane)	0.09	0.09	0.05	0.00	0.00	0.00
C ₁₀ H ₁₀ (methylindene)	0.24	0.13	0.09	0.06	0.00	0.00
C ₁₀ H ₁₀ (dihydronaphthalene)	0.00	0.00	0.00	0.00	0.00	0.00
C ₁₁ H ₁₀ (methylnaphthalene)	0.13	0.15	0.02	0.02	0.02	0.00
coke (est)	48.88	26.44	15.36	16.65	13.95	21.20
CO + CO ₂	8.24	6.17	3.53	0.00	0.00	0.00
olefins	7.79	7.37	4.76	0.70	0.22	0.00
aromatics	11.62	11.61	7.48	0.85	0.31	0.08
deactivation rate (eq 4)		126.0	51.2	23.4	5.5	−9.5
catalyst activity (eq 5)		0.68	0.41	0.24	0.19	0.28
total coke on catalyst (wt coke/wt cat.)	2.98	11.02	22.25	60.77	115.11	269.96

^a Reaction conditions: temperature, 600 °C; furan partial pressure, 6 Torr; and WHSV, 10.4 h^{−1}.

This suggests that the type of coke that is formed inside the zeolite changed with furan conversion. The indane and indenenes were most likely interconverted through a dehydrogenation reaction. The indenenes were converted into aromatics, olefins, and coke, as will be shown later in this paper. Benzofuran was formed by Diels–Alder reaction of two furan molecules. Benzofuran was further converted into CO, aromatics, and coke, as will be shown later in this paper.³⁷ Naphthalene and methylnaphthalene most likely formed coke and hydrogen.

In Table 3, we also grouped the products into CO + CO₂, olefins (including ethylene, propylene, C₄ olefins, allene, cyclopentadiene, hexatriene, and hexadienyne) and aromatics (including benzene, toluene, ethylbenzene, xylene, styrene, benzofuran, indene, naphthalene, methylstyrene, indane, dihydronaphthalene, and methylnaphthalene). The carbon selectivity of aromatics did

not change with increasing furan conversion. However, the CO + CO₂ and olefins increased with increasing furan conversion. This further suggests that the “coke” was larger hydrocarbons that were trapped inside the zeolite at low conversion.

3.5. Effect of Temperature. Table 4 shows the product selectivity for furan conversion as a function of temperature. At 450 °C, benzofuran was the primary product observed.³⁷ The carbon selectivity to benzofuran decreased from 17.7 to 1.7% as the temperature increased from 450 to 650 °C. As the temperature increased, the major products became CO, ethylene, benzene, propylene and toluene. At the higher temperature, the selectivity to highly reactive species, including C₄ olefins, allene, cyclopentadiene, and hexadienyne increased. The selectivity of xylenes, ethylbenzene, methylfuran, furylthylene, and methylindene slightly decreased with increasing temperature. Carbon

Table 3. Carbon Product Selectivity As a Function of Space Velocity^a

WHSV (h ⁻¹)	21.86	10.35	1.95	
furan conversion	0.28	0.48	0.97	
carbon deposited on active sites (mol/mol)	8.97	6.27	1.77	
carbon yield of coke (%)	14.91	14.44	21.56	
products	carbon selectivity (%)			role
CO	11.46	13.91	17.72	product
CO ₂	0.17	1.13	3.30	product
C ₂ H ₄ (ethylene)	6.00	7.40	11.10	product
C ₃ H ₆ (propylene)	4.99	6.71	7.96	product
C ₄ olefins	0.73	0.83	0.79	intermediate
C ₆ H ₆ (benzene)	7.10	8.03	11.60	product
C ₇ H ₈ (toluene)	6.38	7.32	10.69	product
C ₈ H ₁₀ (ethylbenzene)	0.40	0.37	0.11	intermediate
C ₈ H ₁₀ (xylenes)	1.43	1.35	2.72	product
C ₈ H ₈ (styrene)	2.68	2.53	1.42	intermediate
C ₈ H ₆ O (benzofuran)	2.19	1.84	0.25	intermediate
C ₉ H ₈ (indene)	5.19	4.13	2.33	intermediate
C ₁₀ H ₈ (naphthalene)	3.31	2.16	1.14	intermediate
C ₃ H ₄ (allene)	1.39	0.88	0.16	intermediate
C ₅ H ₆ (cyclopentadiene)	3.12	2.71	0.50	intermediate
C ₅ H ₆ O (methylfuran)	1.55	0.86	0.00	intermediate
C ₆ H ₈ (hexatrienes)	0.47	0.32	0.00	intermediate
C ₆ H ₆ (hexadienyne)	0.39	0.26	0.00	intermediate
C ₆ H ₆ O (furylthylene)	0.26	0.16	0.00	intermediate
C ₉ H ₁₂ (trimethylbenzene)	0.00	0.02	0.00	unknown
C ₉ H ₁₀ (methylstyrene)	0.37	0.32	0.14	intermediate
C ₉ H ₁₀ (Indane)	0.57	0.49	0.20	intermediate
C ₁₀ H ₁₀ (methylindene)	1.59	1.36	0.43	intermediate
C ₁₀ H ₁₀ (dihydronaphthalene)	0.12	0.18	0.00	intermediate
C ₁₁ H ₁₀ (methylnaphthalene)	0.77	0.94	0.37	intermediate
coke	37.39	33.80	27.05	intermediate
CO + CO ₂	11.64	15.04	21.03	
olefins	17.08	19.11	20.50	
aromatics	32.09	31.01	31.42	

^a Reaction conditions: 600 °C; furan partial pressure, 6 Torr.

dioxide was observed only at temperatures of 600 and 650 °C. The styrene selectivity went through a slight maximum of 2.5% carbon selectivity at 600 °C. The indene selectivity varied between 3.0 and 4.1% with temperature. The naphthalene selectivity varied between 1.2 and 3.0% with no systematic trend. The coke selectivity decreased with increasing temperature. The olefins and CO + CO₂ selectivity increased with increasing temperature. The selectivity of olefins was less than aromatics at 450–600 °C, but was comparable to aromatics at 650 °C. This indicates that olefins were favorable at high temperatures, but aromatics were favorable at intermediate temperatures. Similar to the WHSV effect, more olefins, CO, and CO₂ were extracted from the retained intermediates at high furan conversion.

3.6. Conversion of Benzofuran and Indene. Benzofuran and indene were identified as two important intermediates. We also fed them into the flow fixed-bed reactor (benzofuran, 99%; indene, 98%; both from Sigma-Aldrich). Their vapor pressures are quite low, making it impossible to feed by a syringe pump. We

Table 4. Carbon Product Selectivity As a Function of Reaction Temperature^a

	reaction temp (°C)			
	450	500	600	650
furan conversion	0.22	0.32	0.48	0.60
CO	6.7	11.5	13.9	17.9
CO ₂	0.0	0.0	1.1	1.1
C ₂ H ₄ (ethylene)	3.9	4.3	7.4	11.4
C ₃ H ₆ (propylene)	2.3	3.8	6.7	7.9
C ₄ olefins	0.1	0.5	0.8	1.4
C ₆ H ₆ (benzene)	3.6	4.9	8.0	9.4
C ₇ H ₈ (toluene)	4.2	5.4	7.3	6.6
C ₈ H ₁₀ (ethylbenzene)	0.7	0.6	0.4	0.2
C ₈ H ₁₀ (xylenes)	1.5	1.3	1.3	0.9
C ₈ H ₈ (styrene)	0.8	1.2	2.5	1.9
C ₈ H ₆ O (benzofuran)	17.7	4.4	1.8	1.7
C ₉ H ₈ (indene)	3.4	3.0	4.1	3.0
C ₁₀ H ₈ (naphthalene)	1.8	3.0	2.2	1.2
C ₃ H ₄ (allene)	0.0	0.1	0.9	2.0
C ₅ H ₆ (cyclopentadiene)	0.1	0.6	2.7	3.7
C ₅ H ₆ O (methylfuran)	1.4	1.3	0.9	0.5
C ₆ H ₈ (hexatrienes)	0.0	0.4	0.3	0.1
C ₆ H ₆ (hexadienyne)	0.0	0.0	0.3	0.3
C ₆ H ₆ O (furylthylene)	0.3	0.3	0.2	0.1
C ₉ H ₁₂ (trimethylbenzene)	0.0	0.1	0.0	0.0
C ₉ H ₁₀ (methylstyrene)	0.2	0.2	0.3	0.6
C ₉ H ₁₀ (Indane)	1.1	1.6	0.5	0.2
C ₁₀ H ₁₀ (methylindene)	2.0	1.3	1.4	0.8
C ₁₀ H ₁₀ (dihydronaphthalene)	0.0	0.0	0.2	0.1
C ₁₁ H ₁₀ (methylnaphthalene)	0.7	0.5	0.9	0.4
coke	47.4	49.7	33.8	26.9
CO + CO ₂	6.7	11.5	15.0	19.0
olefins	6.4	9.7	19.1	26.7
aromatics	37.7	27.3	31.0	26.8

^a Reaction conditions: WHSV, 10.4 h⁻¹; furan partial pressure, 6 Torr.

fed these reactants using a helium carrier gas (408 mL/min) through a bubbler containing benzofuran or indene. The reaction temperature was 600 °C for each run. Table 5 shows the carbon selectivity of products obtained from benzofuran and indene conversion. The major products from benzofuran conversion were CO, benzene, toluene, and coke. These products accounted for 91% of the products. Benzene was the primary aromatic being produced in 41% carbon selectivity. Only trace amounts of olefins were observed (<0.5% for C₂ and C₃ olefins, and 0% for the others). Small amounts of furan (2.0% carbon selectivity) were observed. Other products that were formed in small concentrations (less than 3% carbon selectivity) include indene > styrene > naphthalene > xylenes > methylindene > methylnaphthalene > ethylbenzene. These results indicate that olefins did not form from benzofuran, but were formed from a separate pathway. This also suggests that during furan conversion, olefins and aromatics formed by different reaction pathways. If all the oxygen is removed by decarbonylation, then the CO selectivity should be 12.5%. In our study, we obtained 87% of this value (Table 5, 10.87 of 12.5). This suggests that benzofuran underwent decarbonylation reactions.

Table 5. Carbon Selectivity (%) of Products Obtained by Using Benzofuran or Indene As the Feedstock^a

products	benzofuran	indene
CO	10.87	0.00
C ₂ H ₄ (ethylene)	0.45	5.01
C ₃ H ₆ (propylene)	0.42	1.25
C ₄ H ₄ O (furan)	1.99	0.00
C ₆ H ₆ (benzene)	41.01	16.81
C ₇ H ₈ (toluene)	13.87	9.71
C ₈ H ₁₀ (ethylbenzene)	0.13	1.42
C ₈ H ₁₀ (xylenes)	0.64	1.04
C ₈ H ₈ (styrene)	1.52	4.23
C ₉ H ₈ (indene)	2.81	x
C ₁₀ H ₈ (naphthalene)	0.80	4.10
C ₃ H ₄ (allene)	0.00	0.86
C ₉ H ₁₀ (indane)	0.00	2.76
C ₁₀ H ₁₀ (methylindene)	0.35	1.62
C ₁₁ H ₁₀ (methylnaphthalene)	0.17	0.00
coke	24.98	51.21
CO + CO ₂	10.87	0.00
olefins	0.86	7.11
aromatics	61.30	41.68

^a Reaction conditions: temperature, 600 °C; helium carrier gas, 408 mL/min; *W*_{HZSM-5}, 57 mg; feedstocks were fed by a bubbler.

Indene produced coke (51% carbon selectivity), aromatics (42% carbon selectivity), and olefins (7% carbon selectivity). Benzene, toluene, and styrene were the primary aromatics produced from indene. Ethylene was the primary olefin produced from indene. It produced only ethylene and did not produce any of the higher olefins. It should be pointed out that the ratio of the moles of benzene to moles of ethylene was 1.1. This suggests that ethylene and benzene are made from a common intermediate (possibly by dealkylation of styrene). Trace quantities of indane and methylindene were formed, most likely from hydrogenation and alkylation of indene, respectively. Other products that were observed include ethylbenzene, xylenes, naphthalene, and allene. High yields of coke were observed (>50% coke selectivity), indicating that indene was a coke precursor.

3.7. Identification of Products Inside the Zeolite during Furan Conversion. As described in Section 2.3, we extracted compounds retained inside HZSM-5 during furan conversion using HF and DCM. The products were obtained by running the flow fixed-bed reactor at various temperatures (25–600 °C) at a space velocity (WHSV) of 2.36 h⁻¹. The furan partial pressure was 6 Torr. After 4 min time on-stream, the reactor was quenched to room temperature, followed by the leaching process mentioned in Section 2.3. The 1/20 volumetrically diluted solutions were clear and showed various colors. The solutions after leaching of the zeolite were yellowish for the 500 and 600 °C samples and black for all other samples. The compounds identified by GC/MS are shown in Table 6 with their structures drawn as compounds 1–26 in Table 7. Most of these compounds were oxygenates with conjugated double bonds. However, they contributed to only less than 5% of the overall carbon that was in the zeolite. Volatile organics were lost during the process. In addition, most of the retained compounds were high molecular weight, which cannot be detected using GC. Figure 6

shows the GPC results of the leached solution, showing that the molecular weight of the retained compounds can be as high as 10⁶ (this is explained later in this paper). The concentration of species observed by GPC decreased with increasing temperature, especially for the heavy compounds (short retention time). The negative peak at a *M*_w of 100 g/mol was caused by DCM, which is shown in Figure 7, where pure DCM has a negative peak at the retention time equal to 100 g/mol.

As shown in Figure 8, when increasing temperature, the identified *M*_w distribution moved from high *M*_w to low *M*_w (excluding the negative peak area from the DCM solvent). One explanation for this phenomena is that the retained compounds polymerized with increasing temperature (probably in polycyclic aromatic structures), and we were not able to analyze these polymers, since they cannot be dissolved in DCM. We did see a lot of blackish particles suspended and aggregated in both HF and DCM phases at elevated temperatures, which we were not able to analyze with any technique. At 300 and 400 °C, the furan polymers began to decompose, and oxygen was removed as CO and CO₂. Those retained compounds formed products and unknown intermediates that were insoluble in DCM due to their structure and high molecular weight. At 500 and 600 °C, the furan polymers were converted into gaseous products with only small amounts of soluble products detected in the DCM, as shown in Figure 6. These retained compounds at these temperatures were graphite-type coke that were insoluble in DCM.

Among the retained compounds shown in Tables 6 and 7, furan showed high selectivity at room temperature (42%) and gradually decreased (9.2%) as the reaction temperature increased, as shown in Table 6. Furan and the other oxygenates made up to 80% of the identified carbon by GC/MS at most temperatures. This indicates that the oxygenates were the major species inside the zeolite catalyst. Deoxygenated aromatics (benzene, toluene, naphthalene, and methylnaphthalene) were formed inside the HZSM-5, usually at temperatures higher than 400 °C. They were observed only in trace quantities at temperatures below 400 °C. Benzene and toluene were final products that have been shown in previous results. Benzofuran and dibenzofuran (19) were formed via Diels–Alder condensation. Benzodioxane (13) and 2,2-methylenebisfuran (6) showed the highest selectivity at 300 and 100 °C, respectively. To understand the formation of these compounds will be a future work.

The number of retained carbon per aluminum site was also calculated as shown in Table 6. It decreased with increasing temperature, indicating that less mass was trapped inside HZSM-5 at higher temperatures. In addition to compounds retained inside HZSM-5, we found that there were tars condensed at the outlet of the quartz reactor after reactions at 400–600 °C. Their composition was identified by GC/MS and is shown in Table 6 (compounds 11, 14, 19, and 27–31). Most of them were deoxygenated and were polycyclic aromatics. Their formation was probably due to crackings from heavy intermediates or continued alkylation or dealkylation from aromatics.

The UV–vis spectra of the DCM solutions from leaching of the zeolite–furan mixtures are shown in Figure 9. UV–vis is a good technique to identify conjugated double bonds.^{42,50} At room temperature, strong absorption bands were observed at around 234, 274, and 364 nm. These bands were formed from compounds that have no more than six conjugated double bonds, indicating that they were smaller in size than furan trimers.⁵⁰ A red shift toward more delocalized conjugated double bonds was observed as the temperature of the furan–zeolite mixture

Table 6. Carbon Selectivity of Retained Compounds Obtained from HF Leaching Experiment^a

species	C ₄ H ₄ O	C ₄ H ₈ O	C ₆ H ₆	C ₇ H ₈	C ₈ H ₆ O	C ₉ H ₈ O ₂	C ₆ H ₆ O	C ₉ H ₈ O	C ₁₁ H ₁₂ O ₂	C ₇ H ₈ O	C ₁₀ H ₈	C ₁₀ H ₁₀ O
no.	1	2	3	4	5	6	7	8	9	10	11	12
RT	42.2	0.9	0.0	0.0	8.1	2.0	0.0	0.0	1.2	0.0	0.0	0.0
100	2.3	0.1	0.0	0.0	11.2	14.0	0.0	0.1	0.5	0.0	0.1	0.0
200	3.3	2.3	0.0	0.0	14.7	1.6	0.0	1.3	0.0	0.0	0.7	20.0
300	6.8	2.5	0.4	0.4	4.8	3.3	3.4	1.0	0.0	1.1	0.9	4.6
400	0.1	0.2	0.5	0.0	0.9	2.5	1.1	2.0	0.0	2.8	3.6	2.5
500	7.3	14.6	20.0	10.9	2.6	0.0	0.0	0.0	0.0	0.0	29.7	0.0
600	9.2	48.4	20.2	6.0	0.0	0.0	0.0	0.0	0.0	0.0	13.1	0.0

species	C ₈ H ₈ O ₂	C ₁₁ H ₁₀	C ₁₁ H ₁₀ O ₂	C ₈ H ₈ O	C ₁₂ H ₁₂ O ₂	C ₁₁ H ₈ O	C ₁₂ H ₈ O	C ₁₁ H ₁₄ O	C ₁₀ H ₈ O	C ₁₂ H ₁₀ O ₂	C ₁₁ H ₁₀ O	C ₁₀ H ₈ O ₂
no.	13	14	15	16	17	18	19	20	21	22	23	24
RT	0.0	0.1	3.3	0.0	0.8	0.0	0.0	0.0	0.0	0.0	0.0	0.4
100	0.0	0.1	23.3	0.0	4.5	0.0	0.0	0.0	0.0	2.4	0.0	0.7
200	9.7	0.9	0.0	0.0	5.4	4.0	16.8	0.0	0.0	19.3	0.0	0.0
300	50.3	0.6	0.0	4.3	0.0	0.0	3.7	7.7	4.2	0.0	0.0	0.0
400	3.9	1.7	0.0	1.6	0.0	0.0	0.9	2.3	41.4	0.0	32.0	0.0
500	0.0	7.8	0.0	0.0	0.0	0.0	0.0	0.0	7.2	0.0	0.0	0.0
600	0.0	3.1	0.0	0.0	0.0	0.0	0.0	0.0	0.0	0.0	0.0	0.0

species	C ₁₅ H ₁₄ O ₃	C ₁₂ H ₁₂ O ₃	H/C _{eff}	% identified C	μmol of C/g. cat.
no.	25	26			
RT	14.0	27.2	0.4	5.22	1876
100	32.8	7.8	0.4	4.60	1488
200	0.0	0.0	0.4	0.73	223
300	0.0	0.0	0.5	2.57	605
400	0.0	0.0	0.4	2.09	353
500	0.0	0.0	0.8	0.23	33
600	0.0	0.0	1.1	0.48	49

^a Spent catalyst was obtained from furan conversion over HZSM-5 in the flow fixed-bed reactor. Reaction conditions: WHSV, 2.36 h⁻¹; furan partial pressure, 6 Torr; reaction time, 4 min (see also Table 7).

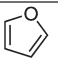
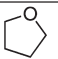
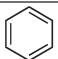
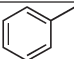
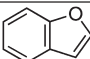
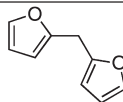
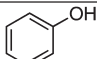
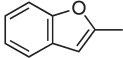
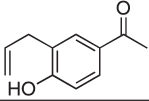
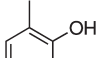
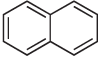
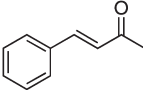
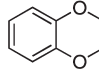
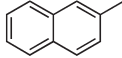
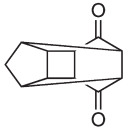
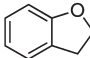
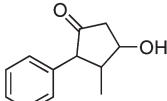
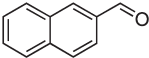
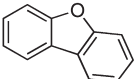
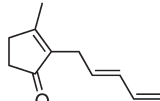
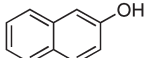
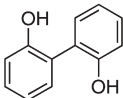
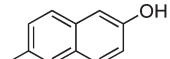
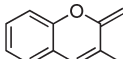
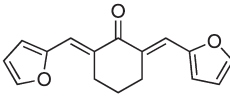
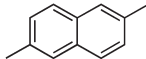
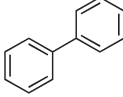
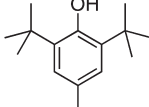
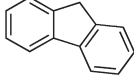
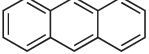
increased from RT to 300 °C which was evidence that the conjugated double bonds grew with increasing temperature inside HZSM-5. The number of conjugated double bonds at 300 °C was much greater than six (close to infinity).^{42,50} The spectra intensity decreased dramatically at 400 °C. This can be explained by the observation that most compounds were converted to gas phase products and insoluble products at this temperature. However, compounds having conjugated double bonds still existed in the DCM solutions and resulted in absorption under UV–vis irradiation. At 500 and 600 °C, the intensity was low, since the produced graphite-type coke was insoluble in DCM. In Table 7, we also found that almost all retained compounds identified by GC/MS have conjugated double bonds. However, although conjugated double bonds were identified by UV–vis and GC/MS, it is not possible to infer correct structures of those compounds.

In addition to condensed phase products, gas phase products were collected in air bags and analyzed by GC/FID. As shown in Figure 10, furan conversion went through a minimum at 400 °C and then increased with increasing temperature. The decrease before 400 °C could be attributed to the blocking of zeolite pores by furan polymers. At 400 °C, gas phase products such as CO, aromatics, and olefins were formed, but the reaction rate was low. At 500 and 600 °C, the reaction routes were shifted to the formation of gas phase products. Compounds that did not diffuse

out formed graphite-type coke. The gas phase products distribution is consistent with TGA–MS and in situ FTIR where products can be formed only at temperatures higher than 400 °C. The slightly restored signal in FTIR representing a Brønsted acid site was attributed to the formation of gas phase products.

It was not possible to identify all retained compounds in the leaching experiments. Most compounds were volatile or insoluble in DCM. In addition, we lost some mass during the HF dissolution process due to the increasing temperature caused by heat of dissolution (exothermic process). The acidic circumstances also caused the polymerization of intermediates. In another test, we added 1 mL of furan into 5 mL of HF and HCl. Then we used 5 mL of DCM to extract organic compounds, and the organic samples were subjected to GPC analysis. Figure 7 shows that furan polymerized in HF and HCl. It is interesting that the furan polymers also showed two different M_w distributions in the strong acid solution (HCl). We repeated the leaching/GPC experiment described in Sections 2.3 and 3.7 by using nonporous silica/alumina as a catalyst. The reactions were run at RT and 300 °C. As shown in Figure 7, the furan was again polymerized and had two major M_w regions. Figure 7 suggests that the existence of compounds that have $M_w \sim 10^6$ probably was due to the limitation of the GPC column (the limitation of the M_w for the GPC column is 10^4), since no matter how we

Table 7. Structures of Identified Retained Compounds (see also Table 6)

1	2	3	4	5	6	7
						
8	9	10	11	12	13	14
						
15	16	17	18	19	20	21
						
22	23	24	25	26	27	
				Unknown, may have $M_w = 204$		
28	29	30	31			
						

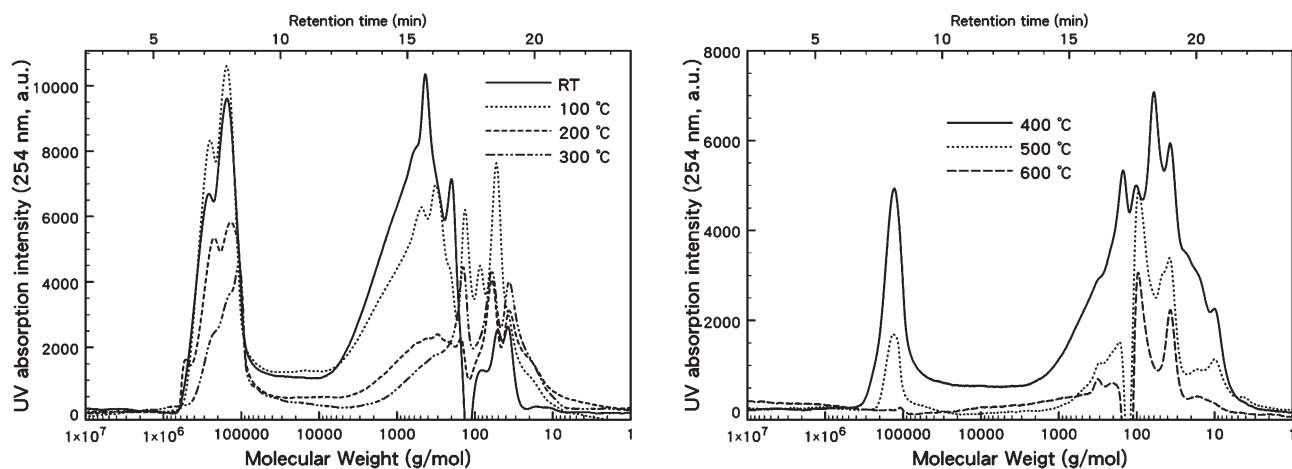


Figure 6. Molecular weight distribution of species inside HZSM-5 during furan conversion at various temperatures. Reaction conditions: WHSV, 2.36 h^{-1} ; furan partial pressure, 6 Torr; reaction time, 4 min.

polymerized furan, it showed $M_w \sim 10^6$ after $\sim 10^4$. We concluded that furan formed polymers that have $M_w (>10^4)$ beyond the limitation of the GPC column.

3.8. Coke Combustion. Figure 11 shows the TPO curves obtained in the combustion of the coke deposited on the catalyst after reactions at different temperatures (25, 300, 400, and 600 °C). Deconvolution of each curve is shown in Table 8 using four different curves with peak temperatures of 523–560, 433–489, 218, and 50 °C. In Table 8, the oxygenated coke means heavy oxygenates retained inside zeolites (e.g., furan polymers). The peaks at temperatures from 523 to 560 °C most likely represented graphitic coke consisting of large polycyclic aromatics.^{25,49} The lower-temperature coke was hydrocarbon

species trapped inside the zeolite or on the pores that probably contained oxygen. As the reaction temperature increased, the TPO curves were shifted to a higher temperature. However, the high-temperature coke formed even when furan was adsorbed at room temperature. This coke contributed almost 50% of the entire coke at room temperature. It was surprising that the graphite-type coke formed at 25 °C, since no CO or CO₂ were observed in the gas phase. At 600 °C, more than 90% coke was graphite-type coke. As shown in Table 8 the highest-temperature deconvolution peak gradually shifted from 523 to 560 °C, and its area ratio increased as the reaction temperature increased. An area ratio drop at 400 °C (0.62 at 300 °C but 0.48 at 400 °C) was found, which was consistent with TGA–MS; FTIR; and the

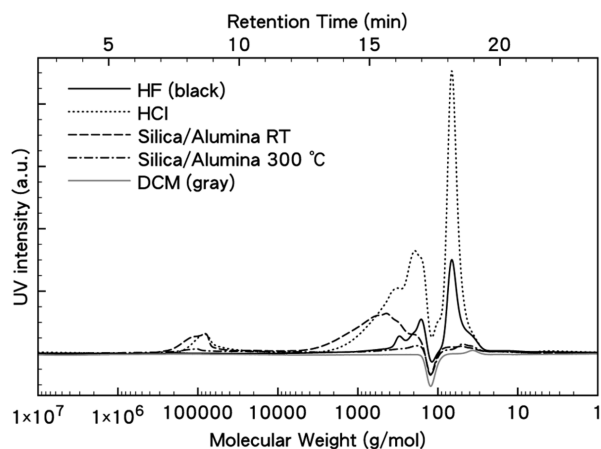


Figure 7. Molecular weight distribution of products obtained by mixing 1 mL of furan with 5 mL of HCl or with 5 mL of HF, and species retained on the silica/alumina (reaction conditions: WHSV, 2.36 h⁻¹; temperatures, 25 and 300 °C; furan partial pressure, 6 Torr), and pure DCM.

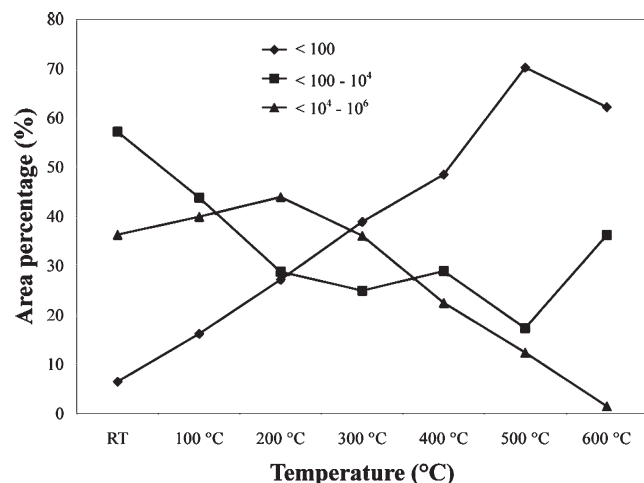


Figure 8. Molecular weight distribution of species inside HZSM-5 during furan conversion. Area ratios of different M_w regions calculated from GPC spectra (Figure 6).

leaching experiment (Figure 10), in which retained oxygenates were decomposed and the gas phase products were produced at 400 °C. The TPO results were evidence that furan formed very heavy oxygenates retained inside HZSM-5, even when furan adsorbed at room temperature.

4. DISCUSSION

4.1. Thermodynamic Consideration. Naphthalene, benzene, toluene, and xylenes produced from furan are highly thermodynamically favored products. This is apparent in Table 9 (reactions 7, 3, 4, and 5, respectively), which shows the Gibbs free energies for stoichiometric reactions to convert furan into monocyclic and polycyclic aromatics.⁵¹ The data in Table 9 show that there is a significant driving force for furan to form both aromatics and olefins at temperatures of 450–600 °C. The aromatics are more thermodynamically favored compared with the olefins. However, the distributions of the products obtained in this study were selective to benzene, toluene, and light olefins.

Table 10 shows that the molar carbon ratios of (benzene + toluene) to (ethylene + propylene) were 0.83–1.28 in all reaction conditions. The thermodynamic calculations also show that toluene is more favorable than benzene. However, more benzene than toluene was produced for furan conversion over HZSM-5.

ASPEN software was also used to calculate the thermodynamic product distribution of furan at different temperatures, as shown in Table 10. We used the built-in thermodynamic data from ASPEN and the Peng-Robinson EOS to do these calculations. Table 10 shows that the product distribution was far from thermodynamic equilibrium. For example, experimental data showed that the benzene/toluene ratios were close to 1, benzene was always more than naphthalene (benzene/naphthalene >1), and the ethylene/propylene ratio was only a little bit higher than 1. However, simulation results showed that benzene/toluene and ethylene/propylene ratios for all temperatures were much greater than 1, and naphthalene was more thermodynamic favorable than benzene (benzene/naphthalene <1). The thermodynamic values for the (B + T)/(E + P) ratio were hundreds of times greater than the experimental results.

One of the most thermodynamically stable compounds from our thermodynamic calculations was naphthalene, which contributed <3.5% carbon selectivity throughout our experiments (except when indene was the feed). Only trace quantities of products larger than naphthalene, such as anthracene, were identified in our study (Table 7). An explanation for the lack of detectable heavy hydrocarbons is that it was the pore size of the catalyst that restricted the products that were produced inside HZSM-5. The GPC result showed that some of the oxygenated intermediates can have a M_w up to 10^4 . Once products heavier than naphthalene formed, they did not diffuse out of the channels because of slow diffusion. The TPO curves and FTIR spectra also showed that graphite-type coke existed inside the HZSM-5 catalyst, especially when the reaction temperature was higher than 400 °C. This space confinement leads the reaction far from thermodynamic equilibrium.

4.2. Diffusion Limitation. It is believed that diffusion of molecules in zeolites plays a central role in reactions and separations.⁵² To elucidate the diffusion in the study, we calculated the Weisz Modulus as shown in eq 6. All the parameters except effective diffusivity, D_e , were obtained directly from the experiment. Previous researchers have studied the diffusivity of benzene and methylbenzenes in zeolites whose results we used to estimate D_e .^{53–60} We could find little information on the diffusion of furan. Therefore, we estimated our diffusion rate as that of benzene and ethylene in HZSM-5. This is probably a valid assumption, since the kinetic diameter of furan is similar to benzene but greater than ethylene.

$$M_w = L^2 \left(\frac{n+1}{2} \right) \left(\frac{r_p \rho_p / C_{As}}{D_e} \right) \quad (6)$$

Ruthven and Kaul⁵⁵ reported the diffusivity of benzene in NaX zeolite (~ 7.4 Å in pore size) to be on the order of 10^{-11} m²/s at room temperature. In their studies, *p*-xylene and naphthalene were also found to have similar diffusivities but were ~ 1 order smaller than benzene. Similar results were obtained by Ulrich et al. at 378 K.⁵⁶ Song et al.⁵⁹ used frequency-response (FR) method to obtain the diffusivity of benzene in silicalite (~ 5.1 – 5.7 Å in pore size), on the order of 10^{-13} m²/s, which was reasonable according to the smaller pore size than NaX. The

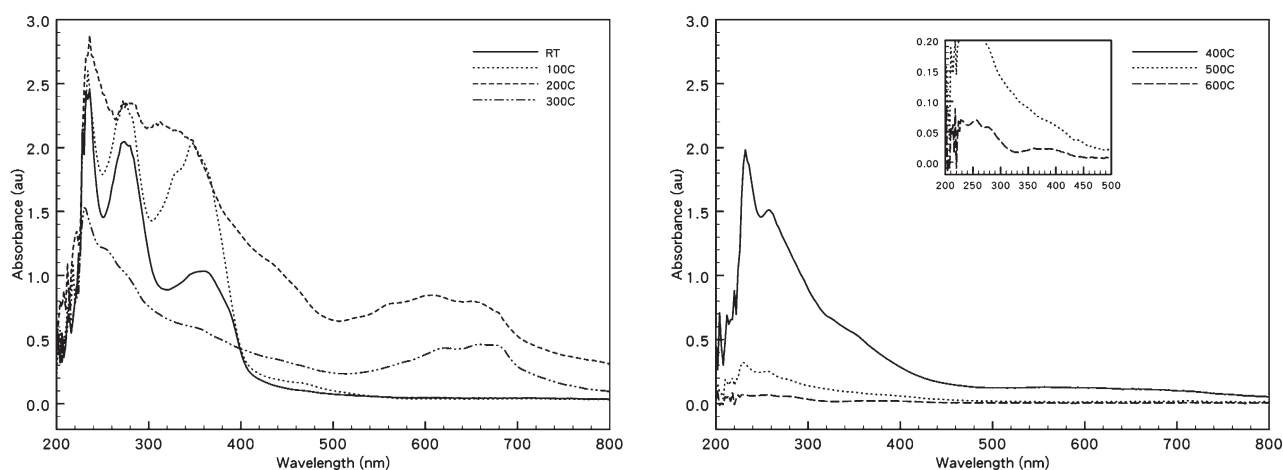


Figure 9. UV-vis spectra of DCM solutions obtained from leaching experiment. For reaction conditions, see Figure 6.

diffusivity of molecules in HZSM-5 (~ 5.5 Å in pore size) is usually a little bit smaller than in silicalite, but it is the same at high temperatures.⁵³ For example, Petryk et al.⁵⁴ modeled the diffusivity of benzene in HZSM-5 at room temperature and obtained a value of 10^{-12} – 10^{-14} m²/s, which was similar to silicalite. Accordingly, we approximately estimated the D_e of benzene in HZSM-5 to be on the order of 10^{-13} – 10^{-14} m²/s; however, diffusivity increases with increasing temperature. The diffusion data obtained by Wu et al.⁵⁷ showed that the diffusivities of benzene and *p*-xylene in silicalite were on the order of 10^{-14} – 10^{-15} , and their temperature dependencies were expressed as Arrhenius relationships. This means that at high temperature, the diffusivity is not sensitive to the change of temperature. Similar results were obtained by Snurr et al., who used transition-state theory to model the benzene diffusion in silicalite.⁵⁸ The temperature-dependency of diffusivity was also found in HZSM-5. Hansen et al.⁵³ used Maxwell–Stefan equations and adsorbed solution theory to model the diffusivities of ethylene and benzene in HZSM-5 and obtained the order of 10^{-11} and 10^{-13} , respectively, at the temperatures 603–703 K.

Here, we used the Arrhenius equation and the data from Hansen to estimate the D_e of benzene in HZSM-5 at 873 K (600 °C). The values we obtained were about 4.8×10^{-12} and 1.2×10^{-11} m²/s for benzene and ethylene, respectively. By substituting into eq 6, we obtained M_w 's that were on the order of 10^7 , suggesting that we had a strong diffusion limitation during reactions. That resulted in the effectiveness ($1/M_w$) of the reaction being close to 0.

Our TPD-MS and in situ FTIR study was probably also in the pore diffusion limited regime according to Gorte et al.^{61,62} However, in our leaching experiment, we found that only when running the reactor at temperatures higher than 400 °C can we see the products (olefins and aromatics, Figure 10). Plus, the UV-vis and GPC spectra (Figures 9 and 6, respectively) showed significant decrease at 400 °C and were attributed to the formation of gas phase products. TPO curves also showed a decrease at 400 °C, suggesting that less mass was accumulated at 400 °C. Moreover, as shown in Figure 3, the in situ FTIR results showed that the OH stretching bands at 3153 and 3125 cm⁻¹ started to decrease at 400 °C. They were all inconsistent with TGA-MS and were evidence that the aromatics and olefins can only be produced at temperatures higher than 400 °C. At lower temperatures, furan

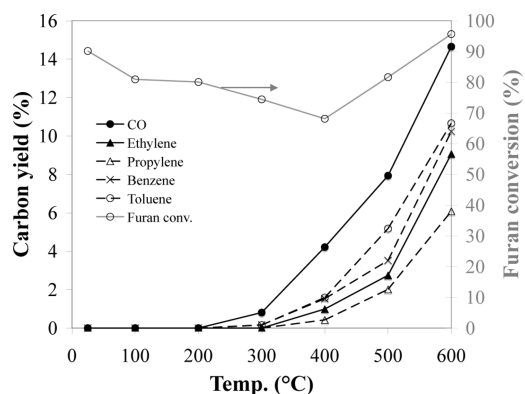


Figure 10. Carbon yield of selected gas phase products obtained from leaching experiment. Furan adsorbed at different temperatures, including room temperature and 100, 200, 300, 400, 500, and 600 °C. Other reaction conditions: WHSV, 2.36 h⁻¹; furan partial pressure, 6 Torr; reaction time, 4 min.

was simply polymerized and was condensed on the HZSM-5 active sites.

4.3. Reaction Mechanism. Many different reactions were occurring for furan conversion inside zeolites. Key reactions that occurred inside the zeolite include Diels–Alder condensation, dehydration, decarbonylation, oligomerization, alkylation, and crackings. In Table 11, we report some of the proposed stoichiometric reactions that occur for furan conversion over HZSM-5. The reactants, intermediates, and products will also be protonated on the HZSM-5 surface.

Furan is a good Diels–Alder condensation source.⁶³ Diels–Alder condensation of furan forms benzofuran and water as reaction 1 in Table 11. High selectivity of benzofuran was observed at low temperatures for furan. The benzofuran can undergo further Diels–Alder reactions with furan to form dibenzofuran and potentially even larger oligomers, which could eventually lead to coke formation (reaction 2). It is likely that the internal pore size of HZSM-5 limits the size of molecules that can form by Diels–Alder reactions. Benzofuran formed lots of CO on HZSM-5, indicating that the rate of decarbonylation was high. We suggest that benzofuran undergoes decarbonylation reactions to form benzene, CO, and coke (Table 5), as shown in reaction 3 in Table 11. No olefins were observed from benzofuran.

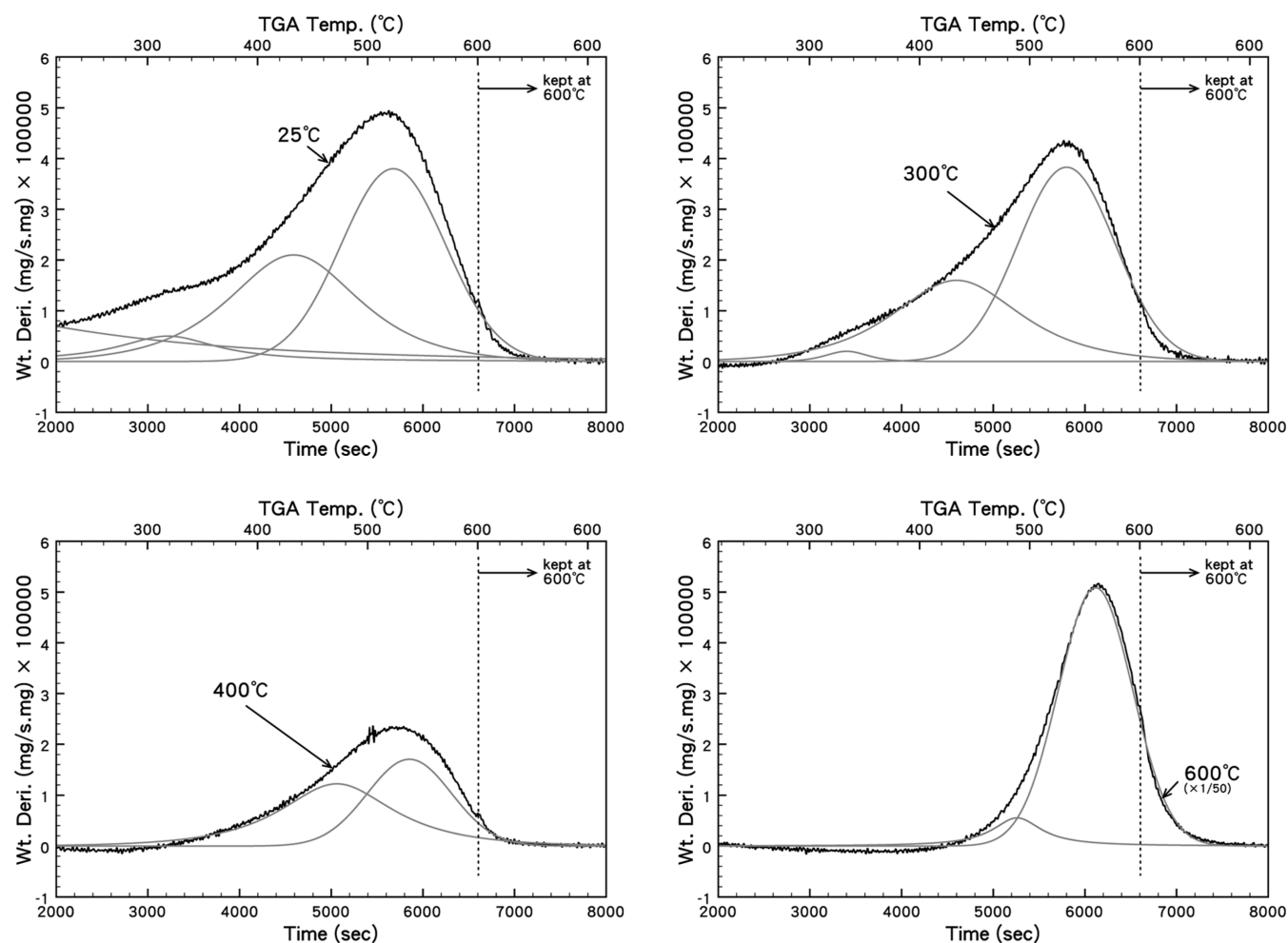


Figure 11. Effect of reaction temperature on the TPO curve for the combustion of the coke deposited on the catalyst. Black, TGA curves; gray, deconvolution curves. Reaction conditions: WHSV = 10.4 h⁻¹; furan partial pressure, 6 Torr; temperature = 25, 300, 400, and 600 °C.

Furan itself can undergo decarbonylation to form allene and CO (reaction 4), which is thermodynamically favorable at 600 °C (Table 9). The first step in the decarbonylation is probably a ring-opening step in which the C–O–C bond is broken on a Brønsted acid site. The unimolecular opening of the furan ring has been reported during furan pyrolysis without catalyst at temperatures higher than 900 °C.^{35,36} Similar to furan, thiophene also undergoes ring-opening over the HZSM-5 catalyst to form olefins.⁴³ Allene undergoes intraconversion between allene and methylacetylene (reaction 4).³⁵ Dehydrogenation of allene to form other olefins can be difficult (Table 9, reaction 10); however, it is an olefin precursor due to its very high reactivity with the existence of acid sites.^{64,65} It has been reported that methylacetylene shows a reaction mechanism similar to propylene over HZSM-5 catalyst where the chain-growth, hydrogen transfer, and crackings on protonated intermediates (carbenium ions) are involved.^{64–66}

In Table 11, we suggest some reactions involving allene to produce olefins, including chain growth, cracking, dehydrogenation, and hydrogen transfer (reactions 5–11). Due to the space confinement imposed by HZSM-5 channels, chain growth of those reactive intermediates leads to cyclization reactions and formation of cyclopentadiene, benzene, and toluene.⁶⁷ Table 9 shows that it is thermodynamically favorable for allene to

Table 8. Deconvolution of TPO Curves in Figure 11

reaction temp (°C)	peak (°C)	ratio	coke type
25	523	0.46	graphite-type
	433	0.34	oxygenated coke
	318	0.07	oxygenated coke
	50	0.12	water or weak adsorption
300	534	0.62	graphite-type
	434	0.01	oxygenated coke
	334	0.37	oxygenated coke
400	538	0.48	graphite-type
	472	0.52	oxygenated coke
600	560	0.91	graphite-type
	489	0.09	oxygenated coke

undergo chain-growth crackings to form other olefins (Table 9, reaction 11) and to react with reactive compounds such as furan and styrene (reaction 12 and 14, respectively).

In this study, we have identified that olefins, especially C₄–C₆ olefins, were intermediates (Table 3). Our results suggested that furan reacted with olefins and formed aromatics and water, as shown in reactions 12–16. In Table 11, furan reacts with

Table 9. Gibbs Free Energy for Furan Conversion into Various Products, Calculated from Data in Ref 51

reaction	temp (°C)	ΔG_{rxn} (kJ/mol)
1 $\text{C}_4\text{H}_4\text{O}$ (furan) \rightarrow C_2H_4 + CO + C	600	-269
	500	-246
	450	-234
2 $2\text{C}_4\text{H}_4\text{O} \rightarrow \text{C}_3\text{H}_6$ + 2CO + H_2 + 3C	600	-380
	500	-351
	450	-336
3 $2\text{C}_4\text{H}_4\text{O} \rightarrow \text{C}_6\text{H}_6$ + 2CO + H_2	600	-304
	500	-276
	450	-262
4 $3\text{C}_4\text{H}_4\text{O} \rightarrow \text{C}_7\text{H}_8$ + 3CO + 2 H_2 + 2C	600	-528
	500	-486
	450	-465
5 $3\text{C}_4\text{H}_4\text{O} \rightarrow \text{C}_8\text{H}_{10}$ + 3CO + C + H_2	600	-464
	500	-434
	450	-418
6 $3\text{C}_4\text{H}_4\text{O} \rightarrow \text{C}_9\text{H}_8$ + 3CO	600	-419
	500	-377
	450	-355
7 $3\text{C}_4\text{H}_4\text{O} \rightarrow \text{C}_{10}\text{H}_8$ + 4CO + 4 H_2 + 2C	600	-615
	500	-565
	450	-539
8 $\text{C}_4\text{H}_4\text{O} \rightarrow 4\text{C} + \text{H}_2\text{O} + \text{H}_2$	600	-280
	500	-270
	450	-266
9 $\text{C}_4\text{H}_4\text{O} \rightarrow \text{CO} + \text{C}_3\text{H}_4$ (allene)	600	-40
	500	-22
	450	-13
10 $2\text{C}_3\text{H}_4 \rightarrow \text{C}_3\text{H}_6$ (propylene) + H_2 + 3C	600	-2
	500	10
	450	15
11 $\text{C}_3\text{H}_4 + \text{C}_3\text{H}_6 \rightarrow \text{C}_2\text{H}_4 + \text{C}_4\text{H}_6$ (C_4 olefins)	600	-40
	500	-41
	450	-42
12 $\text{C}_3\text{H}_4 + \text{C}_4\text{H}_4\text{O} \rightarrow \text{C}_6\text{H}_6$ (benzene) + CO + H_2	600	-264
	500	-254
	450	-250
13 $\text{C}_4\text{H}_4\text{O} + \text{C}_3\text{H}_6 \rightarrow \text{C}_7\text{H}_8$ (toluene) + H_2O	600	-158
	500	-160
	450	-161
14 $\text{C}_8\text{H}_8 + \text{C}_3\text{H}_4 \rightarrow \text{C}_9\text{H}_8$ (indene) + C_2H_4	600	-91
	500	-96
	450	-98

propylene, butyldiene, cyclopentadiene, hexadienyne, and hexatriene and forms toluene, styrene, indene, naphthalene, and methylindene, respectively. The reaction between furan and propylene to form toluene is found to be thermodynamically favorable (Table 9, reaction 13) and has been studied elsewhere.⁸ Under the entire reaction conditions used in this study, ~55% of the C_4 olefins were butadiene. In addition, two different hexatrienes were formed that had a 1:1 carbon ratio. Assume that one

of them helps methylindene formation; thus, the carbon selectivity of olefins decreased as propylene > cyclopentadiene > butyldiene > hexadienyne > hexatriene in most reaction conditions. Looking at reactions 12–16, the olefin selectivity can be used to explain why the aromatic selectivity decreased as toluene > indene > styrene > naphthalene > methylindene. Only reactions at 450 and 500 °C did not follow this rule. For the reaction at WHSV 1.95 h^{-1} , although hexadienyne showed higher selectivity than butyldiene, naphthalene showed higher selectivity than styrene, which means it did not break the rule.

Alkylation reactions also likely occur during furan conversion. The alkylation reactions are thermodynamically favorable (Table 9, reaction 14). Alkylation reactions have been suggested in the hydrocarbon pool mechanism for biomass model compounds reacting on zeolites.^{43,67–70} For example, benzene can be alkylated by ethylene to form ethylbenzene and styrene (if followed by dehydrogenation) on HZSM-5.⁷¹ Chica et al. proposed a mechanism for thiophene conversion over HZSM-5 in which benzothiophene is produced via thiophene alkylation with reactive intermediates (ring-opened thiophene).⁴³ Haw et al. also suggested that during MTO process, alkylation by methanol probably causes chain growth of intermediates.⁶⁷ Methylacetylene can also be polymerized over zeolites (Y, beta, and HZSM-5) to form methylbenzenes.⁶⁵ Propylene is also oligomerized to form aromatics over HZSM-5 catalyst, where adsorbed olefins can undergo Diels–Alder condensation to form cycle olefins and aromatics.^{72,73} In this study, we suggest toluene is continuously alkylated by methylacetylene to form styrene, indene, and naphthalene (reactions 17–19). Benzene can also be alkylated with propylene to form toluene and xylenes (reactions 20 and 21). More alkylated product, trimethylbenzene, was occasionally observed in our experimental conditions.

In addition, alkylation on propylene leads to chain growth and cyclization (reactions 22–24). Ethylene has been considered produced during the formation of aromatics and is involved in mechanisms different from other olefins.⁷⁴ In Table 10, we calculated the molar ratio of ethylene to different aromatics (benzene + toluene + xylenes + styrene + indene + naphthalene) at different reaction conditions. The ratios are close to unity, except for reactions at high WHSV (21.86 h^{-1}) and high temperature (650 °C). This indicates that the formation of aromatics accompanies the production of ethylene. In the study of propylene recycle, we found that propylene cofeed helped formation of alkylated benzenes.⁸ This indicates that alkylation is a possible route to form aromatics. To identify correct reactions about aromatics formation will be a future work.

An HZSM-5 cage that has a hydrocarbon pool and acidic active site inside is viewed as a “supramolecular structure.” It plays an important role during reaction.⁷⁵ Biomass feedstocks can be converted to either intermediates that contribute to the hydrocarbon pool or reactants that provide hydrocarbons to react with the produced hydrocarbon pool and form products. However, the requirement to keep the hydrocarbon pool active is that the feedstock itself should be hydrogen-rich, since the hydrocarbon pool is essentially hydrogen-poor; otherwise, the hydrocarbon pools will grow to form heavy hydrocarbons and coke and block the zeolite channel. During furan conversion, for example, the hydrogen-poor intermediate, methylacetylene, is very easily polymerized to form coke.^{64,65}

In addition, furan itself can be condensed on the HZSM-5 surface via the mechanism similar to benzofuran formation and, finally, form coke. Although the blocked cages still are active for

Table 10. Experimentally Observed and Thermodynamically Calculated Carbon Molar Ratios of Various Products^a

	WHSV (h ⁻¹)	temp (°C)	furan conversion	(B + T)/(E + P),		(B/T), carbon ratio	B/N, carbon ratio	E/(BTXSIN),		
				carbon ratio				molratio		
WHSV effect	1.95	600	0.97	1.17		1.09	10.16	1.28		
	10.34	600	0.48	1.09		1.1	3.72	1.04		
	21.86	600	0.28	0.83		1.43	7.74	1.73		
				Exp	Cal	Exp	Cal	Exp	Cal	
temp effect	10.34	450	0.22	1.27	537	0.86	23	1.95	0.26	0.95
	10.34	500	0.32	1.28	399	0.92	40	1.65	0.23	0.85
	10.34	600	0.48	1.09	247	1.1	98	3.72	0.18	1.04
	10.34	650	0.6	0.83	203	1.43	143	7.74	0.16	1.73

^a P, propylene; E, ethylene; B, benzene; T, toluene; X, xylenes; S, styrene; I, indene; N, naphthalene; Exp, experimentally observed ratio; Cal, thermodynamically calculated ratio. Furan partial pressure: 6 Torr for each run.

Table 11. Suggested Reaction Pathways of Furan Conversion over HZSM-5 at 600 °C

reactions	no.
Diels–Alder Condensation	
2C ₄ H ₄ O (furan) → C ₈ H ₆ O (benzofuran) + H ₂ O	1
C ₄ H ₄ O + C ₈ H ₆ O → C ₁₂ H ₈ O + H ₂ O → ... → coke or heavy oxygenates	2
Decarbonylation of Benzofuran and Furan	
C ₈ H ₆ O → CO + C ₆ H ₆ (benzene) + C (coke)	3
C ₄ H ₄ O → CO + C ₃ H ₄ (allene) = C ₃ H ₄ (methylacetylene)	4
Allene (Methylacetylene) Reactions	
2C ₃ H ₄ → C ₆ H ₈ → C ₃ H ₆ (propylene) + H ₂ + 3C	5
2C ₃ H ₄ → C ₆ H ₈ → C ₅ H ₆ (cyclopentadiene) + H ₂ + C	6
2C ₃ H ₄ → C ₆ H ₈ → C ₆ H ₆ + H ₂	7
2C ₃ H ₄ → C ₆ H ₈ (hexatrienes) → C ₆ H ₆ (hexadienyne) + H ₂ → C ₆ H ₆ (benzene, by cyclization)	8
3C ₃ H ₄ → C ₉ H ₁₂ → C ₇ H ₈ (toluene) + C ₂ H ₄ (ethylene)	9
C ₃ H ₄ + C ₅ H ₆ → C ₈ H ₁₀ → C ₆ H ₆ (benzene) + C ₂ H ₄	10
C ₃ H ₄ + C ₃ H ₆ → C ₆ H ₁₀ → C ₂ H ₄ + C ₄ H ₆ (C ₄ olefins)	11
Furan–Olefins Reaction	
C ₄ H ₄ O + C ₃ H ₆ → C ₇ H ₁₀ O → C ₇ H ₈ (toluene) + H ₂ O	12
C ₄ H ₄ O + C ₄ H ₆ (butyladiene) → C ₈ H ₁₀ O → C ₈ H ₈ (styrene) + H ₂ O	13
C ₄ H ₄ O + C ₅ H ₆ (cyclopentadiene) → C ₉ H ₁₀ O → C ₉ H ₈ (indene) + H ₂ O	14
C ₄ H ₄ O + C ₆ H ₆ (hexadienyne) → C ₁₀ H ₁₀ O → C ₁₀ H ₈ (naphthalene) + H ₂ O	15
C ₄ H ₄ O + C ₆ H ₈ (hexatriene) → C ₁₀ H ₁₂ O → C ₁₀ H ₁₀ (methylindene) + H ₂ O	16
Alkylations	
C ₇ H ₈ + C ₃ H ₄ → C ₁₀ H ₁₂ → C ₈ H ₈ (styrene) + C ₂ H ₄	17
C ₈ H ₈ + C ₃ H ₄ → C ₁₁ H ₁₂ → C ₉ H ₈ (indene) + C ₂ H ₄	18
C ₉ H ₈ + C ₃ H ₄ → C ₁₂ H ₁₂ → C ₁₀ H ₈ (naphthalene) + C ₂ H ₄	19
C ₆ H ₆ + C ₃ H ₆ → C ₉ H ₁₂ → C ₇ H ₈ + C ₂ H ₄	20
C ₇ H ₈ + C ₃ H ₆ → C ₁₀ H ₁₄ → C ₈ H ₁₀ (xylenes) + C ₂ H ₄	21
2C ₃ H ₆ → C ₆ H ₁₂ → C ₄ H ₈ (C ₄ olefins) + C ₂ H ₄	22
C ₄ H ₈ + C ₃ H ₆ → C ₇ H ₁₄ → C ₂ H ₄ + C ₅ H ₁₀ (C ₅ olefins) → C ₅ H ₆ + 2H ₂ (cyclization)	23
C ₅ H ₁₀ + C ₃ H ₆ → C ₈ H ₁₆ → C ₂ H ₄ + C ₆ H ₁₂ → C ₆ H ₆ + 3H ₂ (cyclization)	24

consuming the biomass-derived feedstock (Figure 5, stability test), the only product they produce is coke.^{67,76} Methanol is a hydrogen-rich feedstock (H/C_{eff} ratio is 2) compared with furan (H/C_{eff} ratio is 0.5), and thus, the lives of their hydrocarbon pools are much different from each other. The hydrocarbon pool produced during methanol conversion can last for several hours, since the feedstock, methanol, is essentially a hydrogen-rich

compound.^{60,77} However, in this study, the HZSM-5 deactivated very rapidly (Figure 5). Therefore, the composition of the hydrocarbon pool produced from furan is considered different from that produced from methanol. The TPO results also indicated the hydrogen-poor features on furan. For example, for methanol conversion over HZSM-5 at 450 °C, the TPO curve showed a peak representing catalytic coke at around

510–520 °C;⁴¹ however, furan conversion over HZSM-5 showed the peak at 538 and 560 °C for reactions at 400 and 600 °C, respectively. The higher oxidation temperatures imply more hydrogen-poor characteristics.

5. CONCLUSION

Conversion of furan to aromatics and olefins over HZSM-5 catalyst has been studied. Temperature-programmed analysis (TGA–MS and in situ FTIR) showed that at room temperature, furan formed oligomers on HZSM-5. The furan adsorption uptake was 1.73 moles of furan per mole of Al site. As the oligomers were heated, they underwent a series of reactions, including Diels–Alder condensation, dehydration, decarbonylation, decarboxylation, alkylation, etc., to produce aromatics and olefins at temperatures higher than 400 °C. Graphite-type coke formed during furan conversion. Oxygen was majorly removed via dehydration, decarbonylation, and decarboxylation.

A continuous flow fixed-bed reactor with a HZSM-5 packed bed inside was used to elucidate the chemistry of furan conversion. Coke rapidly formed on the catalyst surface, leading to a decrease in the overall catalytic activity. Carbon monoxide, ethylene, propylene, benzene, and toluene were final products, since their selectivity increased with increasing furan conversion. However, their carbon yield decreased rapidly with time on-stream due to coke deposition. At high furan conversion (0.97), most oxygen was removed by decarbonylation (18% of 25% maximum selectivity). At 450 °C, benzofuran and coke were major products that contributed 60% carbon selectivity. At intermediate temperatures (500–600 °C), the product distribution was selective to aromatics, especially to benzene and toluene. However, at 650 °C, the carbon selectivity of olefins was comparable to aromatics. Olefins were produced mainly from furan instead of benzofuran or other polyring aromatics, which were identified as important intermediates. The leaching experiment showed that furan can form polymers with $M_w \sim 10^4$, but those polymers decomposed and formed products and coke at 400 °C, which was consistent with TGA–MS. Oxygenated aromatics with conjugated double bonds were identified as compounds retained inside HZSM-5. TPO results showed that furan formed a polyring aromatic structure when adsorbed on the HZSM-5 surface. The type of coke that formed on the catalyst surface was a function of the reaction temperature, with more graphitic-like coke forming at higher reaction temperatures.

The benzene/toluene and (B + T)/(E + P) ratios were close to 1 at all reaction conditions, which was much smaller than their thermodynamic calculated ratios. We proposed a mechanism in which the furan molecules diffuse into HZSM-5 channels and are converted to intermediates such as allene by decarbonylation and benzofuran by Diels–Alder condensation. Olefins are produced via oligomerization and crackings of furan, allene, and olefins themselves. Aromatics are produced via alkylation, cyclization, and reactions between olefins and furan. Ethylene is a leaving group when producing aromatics and olefins or is extracted from coke. Oxygen was removed as water, CO, and CO₂ throughout the reaction. A strong pore diffusion limitation was found by Weisz modulus calculation. We concluded that the reaction was far from thermodynamic equilibrium due to space confinement imposed from HZSM-5 channels. This paper shows that zeolite catalysts can be used to convert hydrogen-poor biomass resources into aromatics and olefins.

AUTHOR INFORMATION

Corresponding Author

*Phone: 413-545-0276. Fax: 413-545-1647. E-mail: huber@ecs.umass.edu.

ACKNOWLEDGMENT

This material is based upon work supported as part of the Catalysis Center for Energy Innovation, an Energy Frontier Research Center funded by the U.S. Department of Energy, Office of Science, Office of Basic Energy Sciences under Award no. DE-SC0001004.

REFERENCES

- (1) Lynd, L. R.; Wyman, C. E.; Gerngross, T. U. *Biotechnol. Prog.* **1999**, *15*, 777–793.
- (2) Wyman, C. E. *Annu. Rev. Energy Environ.* **1999**, *24*, 189–226.
- (3) Wyman, C. E.; Dale, B. E.; Elander, R. T.; Holtzapfle, M.; Ladisch, M. R.; Lee, Y. Y. *Bioresour. Technol.* **2005**, *96*, 2026–2032.
- (4) Singh, N. R.; Delgass, W. N.; Ribeiro, F. H.; Agrawal, R. *Environ. Sci. Technol.* **2010**, *44*, 5298–5305.
- (5) Huber, G. W.; Iborra, S.; Corma, A. *Chem. Rev.* **2006**, *106*, 4044–4098.
- (6) Lin, Y. C.; Huber, G. W. *Energy Environ. Sci.* **2009**, *2*, 68–80.
- (7) Carlson, T. R.; Vispute, T. R.; Huber, G. W. *ChemSusChem* **2008**, *1*, 397–400.
- (8) Carlson, T. R.; Cheng, Y.-T.; Jae, J.; Huber, G. W. *Energy Environ. Sci.* **2011**, *4*, 145–161.
- (9) Diebold, J. P.; Scahill, J. W. *Abstr. Pap. Am. Chem. Soc.* **1987**, *193*, 70-CELL.
- (10) Goyal, H. B.; Seal, D.; Saxena, R. C. *Renewable Sustainable Energy Rev.* **2008**, *12*, 504–517.
- (11) Demirbas, A. *Energy Sources, Part A* **2007**, *29*, 753–760.
- (12) Carlson, T. R.; Tompsett, G. A.; Conner, W. C.; Huber, G. W. *Top. Catal.* **2009**, *52*, 241–252.
- (13) Czernik, S.; Scahill, J.; Diebold, J. J. *Sol. Energy Eng. Trans.-ASME* **1995**, *117*, 2–6.
- (14) Adam, J.; Antonakou, E.; Lappas, A.; Stocker, M.; Nilsen, M. H.; Bouzga, A.; Hustad, J. E.; Oye, G. *Microporous Mesoporous Mater.* **2006**, *96*, 93–101.
- (15) Olazar, M.; Aguado, R.; San Jose, M. J.; Bilbao, J. J. *Chem. Technol. Biotechnol.* **2001**, *76*, 469–476.
- (16) Fabbri, D.; Torri, C.; Baravelli, V. J. *Anal. Appl. Pyrolysis* **2007**, *80*, 24–29.
- (17) Fabbri, D.; Fabbri, F.; Falini, G.; Baravelli, V.; Magnani, A.; Torri, C.; Maskrot, H.; Leconte, Y. *Anal. Appl. Pyrolysis* **2008**, *82*, 248–254.
- (18) Aho, A.; Kumar, N.; Eranen, K.; Salmi, T.; Hupa, M.; Murzin, D. Y. *Fuel* **2008**, *87*, 2493–2501.
- (19) Corma, A.; Huber, G. W.; Sauvanaud, L.; O'Connor, P. J. *Catal.* **2007**, *247*, 307–327.
- (20) Chen, N. Y.; Degnan, T. F.; Koenig, L. R. *CHEMTECH* **1986**, *16*, 506–511.
- (21) Vispute, T. P.; Zhang, H. Y.; Sanna, A.; Xiao, R.; Huber, G. W. *Science* **2010**, *330*, 1222–1227.
- (22) Haniff, M. I.; Dao, L. H. *Appl. Catal.* **1988**, *39*, 33–47.
- (23) Adjaye, J. D.; Bakhshi, N. N. *Fuel Process. Technol.* **1995**, *45*, 161–183.
- (24) Adjaye, J. D.; Bakhshi, N. N. *Fuel Process. Technol.* **1995**, *45*, 185–202.
- (25) Gayubo, A. G.; Aguayo, A. T.; Atutxa, A.; Valle, B.; Bilbao, J. *J. Chem. Technol. Biotechnol.* **2005**, *80*, 1244–1251.
- (26) Bridgwater, A. V.; Cottam, M. L. *Energy Fuels* **1992**, *6*, 113–120.
- (27) Sharma, R. K.; Bakhshi, N. N. *Can. J. Chem. Eng.* **1993**, *71*, 383–391.

- (28) Horne, P. A.; Williams, P. T. *Fuel* **1996**, *75*, 1043–1050.
- (29) Horne, P. A.; Williams, P. T. *Fuel* **1996**, *75*, 1051–1059.
- (30) Horne, P. A.; Williams, P. T. *Renewable Energy* **1996**, *7*, 131–144.
- (31) Hoang, T. Q.; Zhu, X. L.; Sooknoi, T.; Resasco, D. E.; Mallinson, R. G. *J. Catal.* **2010**, *271*, 201–208.
- (32) Zhu, X. L.; Lobban, L. L.; Mallinson, R. G.; Resasco, D. E. *J. Catal.* **2010**, *271*, 88–98.
- (33) Hoang, T. Q.; Zhu, X. L.; Lobban, L. L.; Resasco, D. E.; Mallinson, R. G. *Catal. Commun.* **2010**, *11*, 977–981.
- (34) Carlson, T. R.; Jae, J.; Lin, Y. C.; Tompsett, G. A.; Huber, G. W. *J. Catal.* **2010**, *270*, 110–124.
- (35) Lifshitz, A.; Bidani, M.; Bidani, S. *J. Phys. Chem.* **1986**, *90*, 5373–5377.
- (36) Fulle, D.; Dib, A.; Kiefer, J. H.; Zhang, Q.; Yao, J.; Kern, R. D. *J. Phys. Chem. A* **1998**, *102*, 7480–7486.
- (37) Grandmaison, J. L.; Chantal, P. D.; Kaliaguine, S. C. *Fuel* **1990**, *69*, 1058–1061.
- (38) Kraushaar, B.; Kompa, H.; Schrobbers, H.; Schulz-Ekloff, G. *Acta Phys. Chem.* **1985**, *31*, 581–587.
- (39) Carlson, T. R.; Jae, J.; Huber, G. W. *ChemCatChem* **2009**, *1*, 107–110.
- (40) Guisnet, M.; Magnoux, P. *Appl. Catal.* **1989**, *54*, 1–27.
- (41) Valle, B.; Gayubo, A. G.; Aguayo, A. T.; Olazar, M.; Bilbao, J. *Energy Fuels* **2010**, *24*, 2060–2070.
- (42) Spoto, G.; Geobaldo, F.; Bordiga, S.; Lamberti, C.; Scarano, D.; Zecchina, A. *Top. Catal.* **1999**, *8*, 279–292.
- (43) Chica, A.; Strohmaier, K.; Iglesia, E. *Langmuir* **2004**, *20*, 10982–10991.
- (44) Chica, A.; Strohmaier, K. G.; Iglesia, E. *Appl. Catal., B* **2005**, *60*, 223–232.
- (45) Hernandez, V.; Ramirez, F. J.; Zotti, G.; Navarrete, J. T. L. *J. Chem. Phys.* **1993**, *98*, 769–783.
- (46) Sen, S.; Bardakci, B.; Yavuz, A. G.; Gok, A. U. *Eur. Polym. J.* **2008**, *44*, 2708–2717.
- (47) Hoffmann, P.; Lobo, J. A. *Microporous Mesoporous Mater.* **2007**, *106*, 122–128.
- (48) Halasz, I.; Agarwal, M.; Marcus, B.; Cormier, W. E. *Microporous Mesoporous Mater.* **2005**, *84*, 318–331.
- (49) Mores, D.; Stavitski, E.; Kox, M. H. F.; Kornatowski, J.; Olsbye, U.; Weckhuysen, B. M. *Chem.—Eur. J.* **2008**, *14*, 11320–11327.
- (50) Bordiga, S.; Ricchiardi, G.; Spoto, G.; Scarano, D.; Carnelli, L.; Zecchina, A.; Arean, C. O. *J. Chem. Soc., Faraday Trans.* **1993**, *89*, 1843–1855.
- (51) Yaws, C. L. *Chemical Properties Handbook*; 1st ed.; McGraw-Hill: New York, 1998.
- (52) *Handbook of Zeolite Science and Technology*; Auerbach, S. M., Carrado, K. A., Dutta, P. K., Eds.; Marcel Dekker: New York, 2004.
- (53) Hansen, N.; Krishna, R.; van Baten, J. M.; Bell, A. T.; Keil, F. J. *J. Phys. Chem. C* **2009**, *113*, 235–246.
- (54) Petryk, M.; Leclerc, S.; Canet, D.; Fraissard, J. *Catal. Today* **2008**, *139*, 234–240.
- (55) Ruthven, D. M.; Kaul, B. K. *Ind. Eng. Chem. Res.* **1993**, *32*, 2053–2057.
- (56) Ulrich, K.; Freude, D.; Galvosas, P.; Krause, C.; Karger, J.; Caro, J.; Poladli, P.; Papp, H. *Microporous and Mesoporous Mater.* **2009**, *120*, 98–103.
- (57) Wu, P. D.; Debebe, A.; Yi, H. M. *Zeolites* **1983**, *3*, 118–122.
- (58) Snurr, R. Q.; Bell, A. T.; Theodorou, D. N. *J. Phys. Chem.* **1994**, *98*, 11948–11961.
- (59) Song, L.; Sun, Z.; Duan, L.; Gui, H.; McDougall, G. S. *Microporous Mesoporous Mater.* **2007**, *104*, 115–128.
- (60) Mikkelsen, O.; Kolboe, S. *Microporous Mesoporous Mater.* **1999**, *29*, 173–184.
- (61) Demmin, R. A.; Gorte, R. J. *J. Catal.* **1984**, *90*, 32–39.
- (62) Gorte, R. J. *J. Catal.* **1982**, *75*, 164–174.
- (63) Vollhardt, K. P. C.; Schore, N. E. *Organic Chemistry: Structure and Function*, 5th ed.; W. H. Freeman: New York, 2005.
- (64) Pereira, C.; Kokotailo, G. T.; Gorte, R. J. *J. Phys. Chem.* **1991**, *95*, 705–709.
- (65) Cox, S. D.; Stucky, G. D. *J. Phys. Chem.* **1991**, *95*, 710–720.
- (66) Buchanan, J. S.; Santiesteban, J. G.; Haag, W. O. *J. Catal.* **1996**, *158*, 279–287.
- (67) Haw, J. F.; Song, W. G.; Marcus, D. M.; Nicholas, J. B. *Acc. Chem. Res.* **2003**, *36*, 317–326.
- (68) Haw, J. F.; Richardson, B. R.; Oshiro, I. S.; Lazo, N. D.; Speed, J. A. *J. Am. Chem. Soc.* **1989**, *111*, 2052–2058.
- (69) Xu, T.; Haw, J. F. *J. Am. Chem. Soc.* **1994**, *116*, 10188–10195.
- (70) Sassi, A.; Wildman, M. A.; Ahn, H. J.; Prasad, P.; Nicholas, J. B.; Haw, J. F. *J. Phys. Chem. B* **2002**, *106*, 2294–2303.
- (71) Hansen, N.; Brueggemann, T.; Bell, A. T.; Keil, F. J. *J. Phys. Chem. C* **2008**, *112*, 15402–15411.
- (72) Bhan, A.; Delgass, W. N. *Catal. Rev.—Sci. Eng.* **2008**, *50*, 19–151.
- (73) Ono, Y. *Catal. Rev.—Sci. Eng.* **1992**, *34*, 179–226.
- (74) Bjorgen, M.; Svelle, S.; Joensen, F.; Nerlov, J.; Kolboe, S.; Bonino, F.; Palumbo, L.; Bordiga, S.; Olsbye, U. *J. Catal.* **2007**, *249*, 195–207.
- (75) Haw, J. F.; Marcus, D. M. *Top. Catal.* **2005**, *34*, 41–48.
- (76) Svelle, S.; Ronning, P. O.; Olsbye, U.; Kolboe, S. *J. Catal.* **2005**, *234*, 385–400.
- (77) Aguayo, A. T.; Gayubo, A. G.; Castilla, M.; Arandes, J. M.; Olazar, M.; Bilbao, J. *Ind. Eng. Chem. Res.* **2001**, *40*, 6087–6098.